DESIGN, SYNTHESIS AND CHARACTERIZATION OF MULTIFUNCTIONAL REDOX-RESPONSIVE PORPHYRIN-BASED POLYSILSESQUIOXANE NANOMATERIALS FOR PHOTODYNAMIC THERAPY

by

Daniel Lee Vega

A thesis submitted to the faculty of
The University of North Carolina at Charlotte
in partial fulfillment of the requirements
for the degree of Master of Science in
Chemistry

Charlotte

2015

Approved by:

_____
Dr. Juan Vivero-Escoto

_____
Dr. Craig Ogle

_____
Dr. Michael Walter

_____
Dr. Nathaniel Fried

ABSTRACT

DANIEL LEE VEGA. Design, synthesis and characterization of multifunctional redox-responsive porphyrin-based polysilsesquioxane nanomaterials for photodynamic therapy. (Under the direction of Dr. JUAN L. VIVERO-ESCOTO)

Photodynamic Therapy (PDT) is a minimally invasive clinically approved cancer treatment that was first applied in the early 20th century. PDT is an attractive alternative when compared to chemotherapy and radiation therapy due to the lack of harmful side effects associated with these modalities. This treatment is based on the therapeutic effect of reactive oxygen species (ROS) generated after irradiation to activate a light-sensitive molecule called a photosensitizer (PS). Despite the advantages of PDT for cancer treatment, there are some drawbacks with current PS molecules such as inadequate energy absorption, poor solubility in water, and the inability to target tumor cells. Nanoparticles (NPs) are promising materials to be utilized for PDT. NPs have the ability to be target-specific towards tumor tissue, biocompatible and biodegradable. However, current nanocarriers do not show the optimal PDT response due to self-quenching and low singlet oxygen generation. The main target of this project is to develop stimuli-responsive hybrid nanoparticles based on tetrakis(carboxy)phenyl porphyrin (TCPP) derivatives with an enhanced ability to carry and deliver large amount of PSs to improve the PDT effect. This platform will be further functionalized with polyethylene glycol (PEG) and a targeting ligand, Folic acid (FA) to improve its biocompatibility and target specificity.

DEDICATION

I would like to dedicate this to all my family, friends and loved ones. I could not have done this without your support. The motivation to strive for greatness and never quit has kept me going throughout my academic career and will continue to inspire me to achieve new heights never before imagined. Thank you to those who have given me courage and knowledge to pursue my dreams when it did not seem possible. This is but a glimmer of what the future has in store for me and I am excited to see what is next! “Life is like riding a bicycle. To keep your balance, you must keep moving.” –Albert Einstein

ACKNOWLEDGMENTS

First and foremost, I would like to thank Dr. Juan Luis Vivero-Escoto for his financial support, guidance and mentorship throughout my tenure in the V-lab. Much thanks to my committee members, Dr. Craig Ogle for his instruction in chemistry and words of wisdom, Dr. Michael Walter for his knowledge and expertise in the field of porphyrins and Dr. Nathaniel Fried for his contributions in the field of optics. Thank you, Dr. Richard Jew for being a great friend and guide throughout the years, Dr. Jerry Troutman for your words of inspiration, Dr. Kathryn Asala for assisting me with acquiring financial support as a chemistry student, The UNC-Charlotte Department of Chemistry, UNC-Charlotte Department of Biology and UNC-Charlotte Department of Physics and Optics.

TABLE OF CONTENTS

LIST OF ABBREVIATIONS		viii
CHAPTER 1: INTRODUCTION		1
1.1	Photodynamic Therapy (PDT)	1
1.2	Principles of PDT	1
1.3	History of PDT	3
1.4	Oncological Applications of PDT	3
1.5	Light	4
1.6	Oxygen	5
1.7	Photosensitizers (PS)	6
1.8	Nanoparticle-based PS Delivery Systems for Oncological Applications of PDT	11
1.9	Degradable Hybrid NPs to Enhance the PDT Effect	13
1.10	Research Objective	17
CHAPTER 2: EXPERIMENTAL		23
2.1	Synthesis and Characterization of Folic Acid-Polyethylene Glycol-Amine (FA-PEG-NH_2) and Methoxy-Polyethlyene Glycol-Amine (MeO-PEG-NH_2)	23
2.2	Synthesis and Characterization of Control Tetrakis(Carboxy) Phenyl Porphyrin (C-TCPP) and Redox-Responsive Tetrakis(Carboxy)Phenyl Porphyrin Silane Derivatives	27
2.3	Synthesis and Characterization of TCPP Loaded Multifunctional PSilQ NPs with Target-Specific Capabilities Toward Cancer Cells	35
CHAPTER 3: RESULTS AND DISCUSSION		38
3.1	Synthesis of FA-PEG-NH_2 and MeO-PEG-NH_2	38
3.2	Synthesis of C-TCPP and RR-TCPP	39

3.3 Determination of Singlet Oxygen Generation 44

3.4 Synthesis of C-TCPP and RR-TCPP PSilQ NPs 46

3.5 Conjugation of FA-PEG-NH_2 and MeO-PEG-NH_2 to C-TCPP and RR-TCPP PSilQ NPs 48

CHAPTER 4: CONCLUSION AND FUTURE WORK 51

REFERENCES 55

APPENDIX:FIGURES 63

LIST OF ABBREVIATIONS

$^3O_2$	Triplet-state oxygen
$^1O_2$	Singlet-state oxygen
5-ALA	5-Aminolevulinic acid
C	Control
CPP	Cell-penetrating peptide
DMAP	4-Dimethylaminopyridine
EDC	1-Ethyl-3-(-3-dimethylaminopropyl) carbodiimide
EU	European Union
FA	Folic acid
FDA	Food and Drug Administration
FTIR	Fourier transform infrared spectroscopy
HOMO	Highest Occupied Molecular Orbital
HpD	Hematoporphyrin
NMR	Nuclear magnetic resonance
NP	Nanoparticle
PDT	Photodynamic Therapy
PEG	Poly(ethylene) glycol
PpIX	Protoporphyrin IX
PS	Photosensitizer
PSilQ	Polysilsesquioxane
RR	Redox-responsive
ROS	Reactive Oxygen Species

SE	Succinimide Ester
SEM	Scanning Electron Microscopy
SiNP	Silica Nanoparticle
TCPP	Tetrakis(carboxy)phenyl Porphyrin
TGA	Thermogravimetric Analysis
THF	Tetrahydrofuran

CHAPTER 1: INTRODUCTION

1.1 Photodynamic Therapy

In 2015, there will be an estimated 1,658,370 new cancer cases around the globe. Cancer is responsible for 1 out of 4 mortalities in the United States and is the second leading cause of death behind cardiovascular disease. This year nearly 600,000 Americans cancer patients will die from the disease.[1] Current treatments consist of surgery, chemotherapy, radiation and hormone therapy depending on the type and stage of the cancer. If detected early the patient has a higher probability of survival. Current treatments typically result in major side effects such as pain from treatment, fatigue, hair loss, nausea and anemia. Others include suppression of the immune system, osteoporosis, cardiotoxicity, infertility and pulmonary dysfunction. These effects may last months or even years after the treatments have ended. The current cancer therapies lack specificity to tumor tissue which can harm healthy and cancer tissue alike. Over the decades, much effort from the scientific community has been invested into the development of more specific and effective cancer treatments. This has opened up the door for novel alternatives including, but not limited to photothermal, photodynamic, gene and protein therapies.[2]

1.2 Principles of Photodynamic Therapy

PDT is based on the therapeutic effect of singlet oxygen ($^1O_2$) or reactive oxygen species (ROS) generated after irradiation at an appropriate wavelength and intensity to activate a light-sensitive molecule called a photosensitizer (PS) (Figure 1).[3,4] Ideally,

once the photosensitizer has been administered, it is allowed to accumulate in the target tissue for a certain period of time followed by localized illumination toward the tumor area (Figure 2).[5]

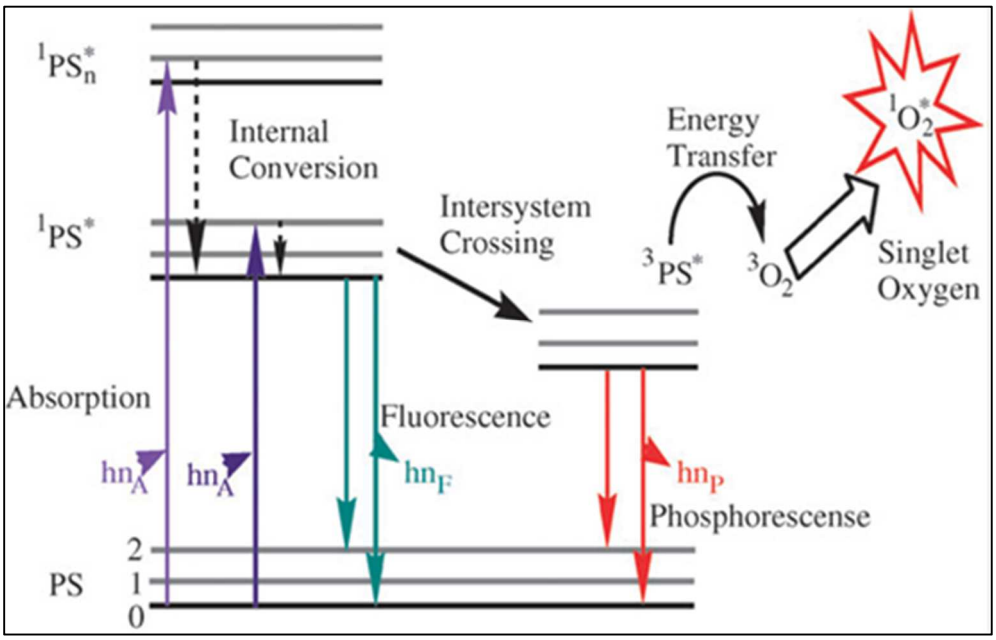

Figure 1: Jablonski diagram depicting the photophysical process for the formation of $^1O_2$.[6]

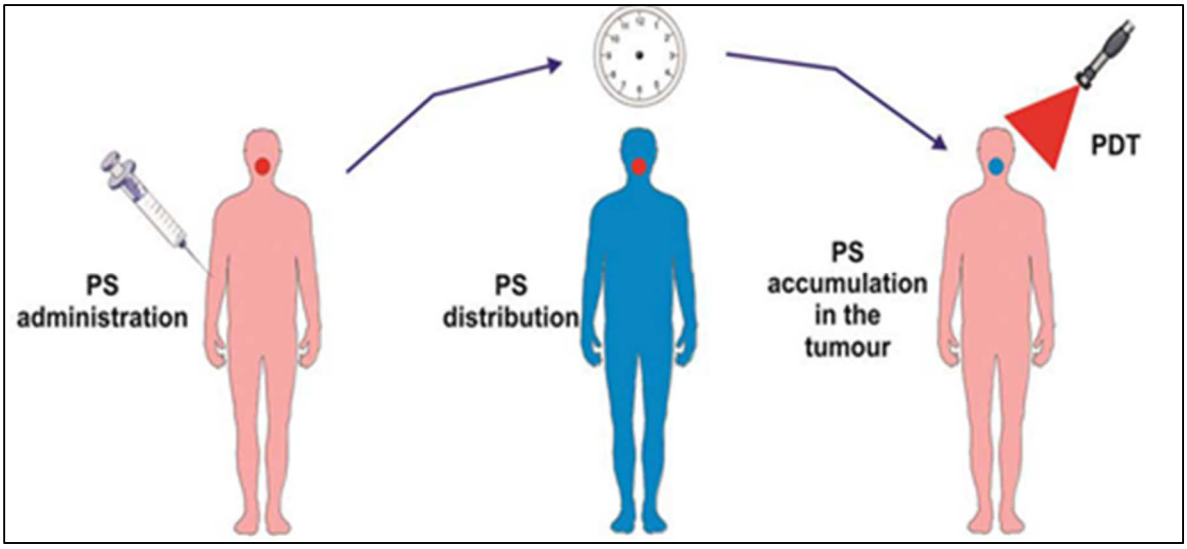

Figure 2: A schematic representation of how current PDT treatments are applied. The PS are administered (left), ideal accumulation in the tumor after an allotted period of time (center), irradiation with light to generate singlet oxygen which leads to cell death.[6]

1.3 History of PDT

The use of light as a therapeutic method has been around for millennia dating back to ancient Egypt, China, India and Greece where it was used to treat cancer, skin diseases and psychosis.[7] Photodynamic Therapy (PDT) is a minimally invasive clinically approved cancer treatment that was first applied in the early 20th century by Niels Finsen to treat smallpox and cutaneous tuberculosis, where he was awarded the Nobel Prize for his work in 1903.[8,9] The term PDT was coined in 1904 by Hermann von Tappeiner.[10] Although, it was not until 1975 when Thomas Dougherty successfully treated skin cancer in patients that PDT gained recognition as an alternative treatment for cancer.[11] In addition to treating cancer and pre-cancerous conditions, PDT has an expansive range of applications such as ophthalmology, localized infections and arterial disease.[12]

1.4 Oncological Applications in PDT

PDT is an attractive alternative to treat cancer when compared to chemotherapy and radiation therapy due to the absence of the above mentioned harmful side effects associated with these modalities. In many cases, surgery cannot be performed as a result of the location of the tumor or age of the patient, whereas PDT can accurately target the tumor site.[13] This treatment works via administration of the photosensitizer systemically, locally or by topical application with the benefit of repeated doses without total dose limitations associated with traditional treatments, and the healing process results in minimal scarring.[14,15] Since the first use of PDT for skin cancer treatment four decades ago, this therapy has been expanding its scope of applications. For example, PDT was first approved for the treatment of bladder cancer in Canada in 1993 using the

photosensitizer, Photofrin®. This photosensitizer was approved by the U.S. Food and Drug Administration (FDA) for esophageal cancer in 1995, lung cancer in 1998 and Barrett's esophagus in 2003.[16,17]

1.5 Light

The ideal range of wavelengths for the light to achieve maximum penetration in tissue and achieve optimal PDT effect are between 650-800 nm.[18] There are two main reasons for this range; the first one deals with hemoglobin, which is one of the main components of blood (red blood cells). This biomolecule contains a porphyrin that absorbs light up to 650 nm. Therefore, hemoglobin will "compete" for the light with porphyrin-based PSs. In principle, longer wavelengths (> 800 nm) of light allow for deeper penetration in tissue. However, in the case of PDT, the PS molecule needs to absorb enough energy to go from the singlet to the triplet state and transfer that energy to activate oxygen. The wavelength for the triplet oxygen to be activated to the singlet state is around 1100 nm. Nevertheless, due to losses of energy from vibrations and heat, the wavelength that the PS molecule needs to absorb is at least 800 nm.[19,20] The depth of skin penetration depends on the wavelength of light used. Light will penetrate up to 5 mm using 630 nm and 1-2 cm with light between 700-800 nm. The use of lasers as a light source for PDT is common in clinical applications. The most commonly used system is the diode laser delivering 1-7 W at 630 nm. Another source of light are the gold or copper vapor lasers that exhibit similar output without the difficulty associated with transporting or cooling the equipment. Traditionally, these systems are used but the downsides are cost of equipment and the need for consistent maintenance.[21,22]

1.6 Oxygen

Molecular oxygen ($^3O_2$) naturally occurs in the triplet ground state with two unpaired electrons with the same spin distributed in the highest occupied molecular orbitals (HOMO). It becomes excited to a singlet state ($^1O_2$) where the two electrons are paired or the electrons have different spins in the HOMO after it reacts with an excited PS. The orbitals of the triplet ground state are depicted versus the singlet excited states of oxygen (Figure 3). The average lifetime of $^1O_2$ is estimated to be between 10-180 ns in biological systems. This lifetime correlates to a diffusion of less than 50 nm per second within cells. Thus, $^1O_2$ cannot diffuse beyond a single cell's thickness because most cells are between 10-100 μm in size. The highly reactive $^1O_2$ will interact with biological molecules such as lipids, proteins and nucleic acids inducing oxidation, which will ultimately result in destruction of the tumor cell via apoptosis, necrosis or autophagy. ROS can also be generated from the interaction between $^1O_2$ and aqueous environments. These include hydrogen peroxide, superoxide, along with peroxyl and hydroxyl radicals. ROS also exhibit oxidative properties and are harmful to cancer cells.[23-27]

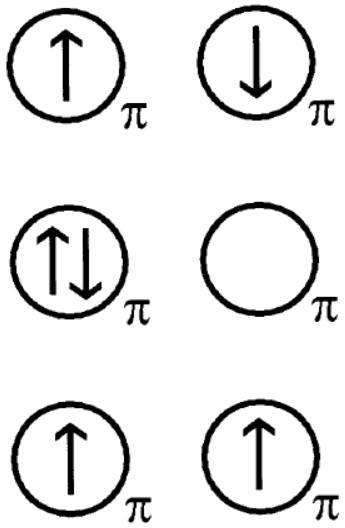

Figure 3: Representation of molecular oxygen lowest singlet and triplet states. Two electrons with the same spin are unpaired in the ground state. Two electrons with opposite spins can either be paired or unpaired in the singlet excited states.[24]

1.7 Photosensitizers

For PDT applications, a PS is a molecule that can be excited by light to produce singlet oxygen and ROS, which causes cell death. Ideally, PSs should be chemically pure, have efficient singlet oxygen generation, possess selectivity for tumor tissue and absorb wavelengths of light that allow maximum skin penetration (650-800 nm). Currently, the PSs used in clinical and experimental studies are derived from naturally occurring tetrapyrrole macrocyclic aromatic pigments such as heme, chlorophyll and bacteriochlorophyll.[28] These pigments are responsible for making blood red, plants green and some bacteria purple.[29] The basic organic structures of photosensitizers include porphyrins, pthalocyanines, chlorins, bacteriochlorins, and other tetrapyrrolic derivatives (Figure 4).[30-32] Photosensitizers are generally classified as porphyrin or non-porphyrins. The word porphyrin arises from the Greek word *porphura* meaning purple.[33]

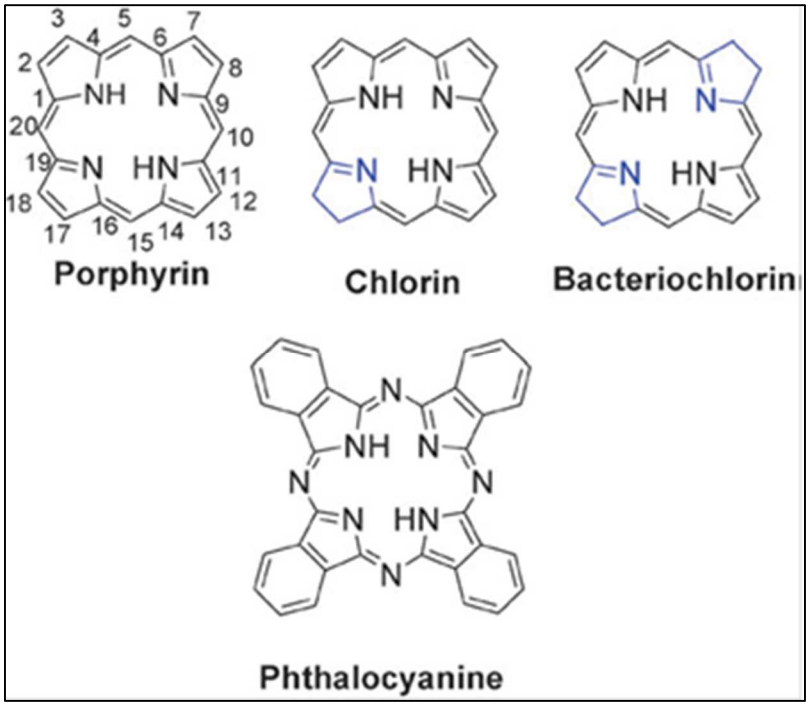

Figure 4: Representative examples of basic organic structures for PSs.[30-32]

PSs have been evolving during the last decades. Molecules with more efficient $^1O_2$ generation, longer absorption wavelengths and target-specific properties have been developed. One way to classify these new PSs is by categorizing them as first, second and third generation (Figure 5).

1.7.1 First Generation Photosensitizers

First generation PSs include Hematoporphyrin derivative (HpD) and Photofrin®. HpD was first developed and studied in the 1960s by Lipson and Schwartz. It was found that HpD had the ability to selectively accumulate in tumors; by utilizing its photophysical properties, it was used as a diagnostic tool. In 1972, Diamond used HpD to treat cancer in mice. The tumors exhibited regression after irradiation with white light. By the end of the decade, Dougherty was successful in the removal of malignant tissues in patients with cancer using HpD.[34-36] Photofrin®, also known as Porfimer sodium or

dihematoporphyrin was the first approved PS for PDT clinical trials. It is a purified version of HpD consisting of a mixture of oligomeric compounds with a maximum absorption wavelength at 630 nm and a relatively low molar absorptivity ($\varepsilon = 3.0 \times 10^3$ M^{-1} cm^{-1}). The drug is administered intravenously at 2-5 mg/kg with light exposure of 100-200 J cm^{-2} for 24-48 hours post injection. Prolonged photosensitivity is an issue due to the long clearance time of 4-12 weeks after injection.[34-38] Another drawback with first generation PSs is the poor depth of tissue penetration due to the low absorbance in the ideal window for PDT (650-800 nm). Therefore, the therapeutic effect depends on large doses of PS and light which can produce harmful side effects.

1.7.2 Second Generation Photosensitizers

To overcome the shortcomings of first generation PSs such as poor solubility in biological systems, a different variety of PDT agents were developed. Second generation PSs generate higher amount of singlet oxygen/reactive oxygen species and absorb at longer wavelengths (red-shifted), which increases the light penetration in tissue; therefore allowing deeper tumors to be targeted.[39] Moreover, these PSs are chemically pure compared with the mixtures of oligomers found in first generation PSs. This new class of PS agents opened up the door for increasing the efficacy of PDT and allowing for the treatment of various types of cancer.[40] Two representative examples of second generation PS molecules are Foscan® and Levulan®. Foscan®, also known as Temoporfin or mTHPC (meso-tetra-3-hydroxyphenyl-chlorin) was first synthesized by Bonnnet in the 1980s. This PS was first approved for head and neck cancer treatment. It has a maximum absorption wavelength at 652 nm with a much higher molar absorptivity ($\varepsilon = 3.0 \times 10^4$ M^{-1} cm^{-1}). The PS is administered intravenously at dosages as low as 0.10-0.15 mg/kg with

light exposure 10-20 J cm^{-2} for 24-96 hours post injection.[41,42] Unfortunately, prolonged photosensitivity is still an issue, but with much shorter time usually lasting 2-4 weeks until complete excretion.[43] Levulan®, also known as δ-aminolevulinic acid or 5-aminolevulinic acid (ALA) is a prodrug that is enzymatically converted to the endogenous molecule, Protoporphyrin IX (PpIX). PpIX also works as PS agent and was FDA approved in 2000 for the treatment of actinic keratosis. PpIX is a naturally occurring porphyrin and is produced in the body by the conversion of the prodrug 5-aminolevulinic acid in the heme biosynthetic pathway once internalized by cells.[44,45] ALA is water soluble allowing for administration of the prodrug systemically, locally and orally with doses of 20 mg/kg. Light exposure occurs for 3-6 hours post administration at 100 J cm^{-2}. PpIX has a maximum absorption wavelength at 635 nm with a relatively low molar absorptivity ($\varepsilon = 5.0 \times 10^3\ M^{-1}\ cm^{-1}$). A drawback of ALA is its hydrophilic character which limits the ability to be internalized by cells. Therefore, a methyl ester version of ALA was developed. Methyl aminolevulinate (MAL), commercially available as Metvix® is approved for the treatment of actinic keratosis in the European Union (EU). The addition of an alkyl group attached to ALA results in higher lipophilicity allowing for increased membrane penetration. The endogenous PpIX generated from these two formulations can be cleared from the body within 24-48 hours.[46-48] Second generation PS agents show advancements in the field of PDT but still lack direct targeting capabilities, near-infrared (NIR) absorption with high molar absorptivity and efficient phototoxic effects at the tumor site.

1.7.3 Third Generation Photosensitizers

Third generation PS agents are an emerging class that is currently under development. Some of the advantages of these types of PSs are: 1) enhanced solubility and 2) greater selectivity and specificity for malignant tissues. Third and second generation PSs have been conjugated to carrier biomolecules that deliver the cargo directly to the tumor area. These biomolecules include, but are not limited to, low density lipoproteins (LDLs), sugars, peptides, polymers, biomolecules and antibodies.[49-52] For example, tetrakisphenyl porphyrin (TPP) conjugated to cell penetrating peptides (CPPs) such as the HIV-1 Tat basic domain sequence, GRKKRRQRRR displayed an increase in cellular uptake both *in vitro* and *in vivo* when compared to unconjugated PSs.[53] In another study, Chlorin was conjugated to the antibody, IgG and exhibited higher phototoxic effects in vitro than unconjugated Chlorin.[54] In recent years, the use of NPs as delivery systems for PSs has attracted great attention. This approach can overcome some of the main issues with first, second and third generation PSs. The following section will describe in detail some of the novel applications of nanotechnology for PS delivery to improve PDT.

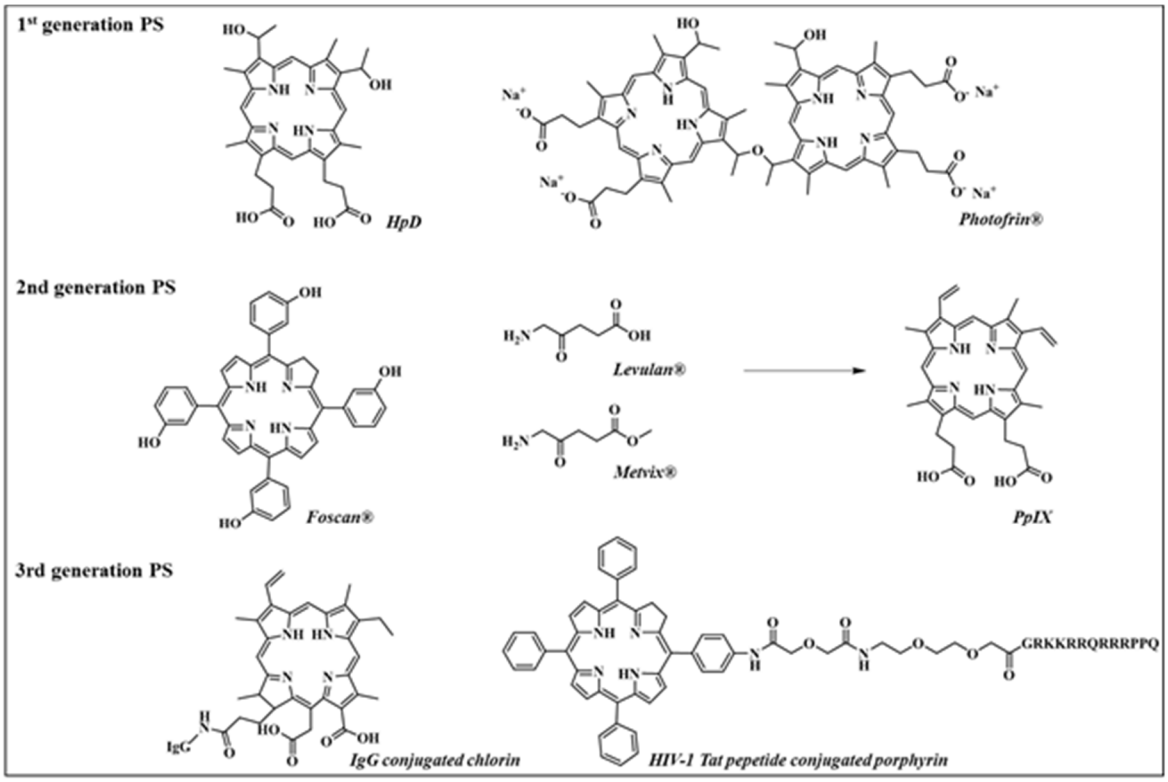

Figure 5: Photosensitizers can be categorized, depending on their properties as first, second or third generation for PDT applications.

1.8 Nanoparticle-based Photosensitizer Delivery Systems for Oncological Applications in PDT

Nanoparticle(NP)-based PS delivery systems are an excellent alternative to improve the performance of PS agents in PDT. Several criteria must be taken into consideration in order to design the optimal vehicle for PS delivery. These include, but are not limited to, size and shape, biocompatibility, biodegradability, PS loading efficiency, ζ-potential, controlled release and the ability to actively target tumor tissue.[55,56] For optimal oncological applications, the size of nanomaterials must be between 20-200 nm in size. NPs less than 20 nm are rapidly cleared by the kidney and excreted through the urinary tract. NPs larger than 200 nm are more readily taken up by macrophages from the immune system. Furthermore, NPs tend to selectively accumulate

in solid tumor through a process called the enhanced permeability and retention (EPR) effect. This phenomenon is due to the chaotic growth of the tumor where the normal vasculature cannot supply sufficient oxygen to the proliferating cells. This results in the rapid formation of vessels that often have irregular structures such as a discontinuous epithelium. Due to these leaky vasculature fenestrations NPs within the ranges of 20-200 nm have shown higher accumulation at the tumor site.[57-60] Some examples of current NP-based platforms for PS delivery include liposomes, gold NP, organic polymers and inorganic materials.[61,62] Several advantages have been demonstrated by using these systems such as target specificity, biocompatibility, biodegradability, and protection of PS until delivery. However; some issues still remain such as premature release of PS, low PS loading, PS self-quenching, and short blood circulation times. In particular the balance between increasing the amount of PS agents inside the nanoparticles and reaching an efficient phototoxic effect has been challenging. The increase of PS content inside NPs usually leads to the aggregation of PS molecules due to their hydrophobic nature, which results in minimal generation of $^1O_2$ due to self-quenching.[19] Different approaches have been explored to overcome these issues. For example, polymeric micelles were used to encapsulate PpIX as an alternative means to deliver the PS. These nanomaterials had the ability to load 4% (wt/%) with a size on the scale of 30 nm measured by dynamic light scattering (DLS). This formulation was tested with H2009 lung cancer cells and displayed relatively low dark toxicity and high PDT efficacy. In another approach, second generation PS, Zinc(II) phthalocyanine (ZnPc) was loaded in mesoporous silica NPs (MSNs) for PDT applications. Scanning electron microscopy (SEM) and transmission electron microscopy (TEM) revealed MSNs with an average size

of 50 nm. The amount of ZnPc content loaded into the pores was 0.8% (wt%). This platform was tested *in vivo* and displayed high tumor specificity and therapeutic efficacy.[63,64] These approaches have shown promising results to improve the performance of PSs for PDT; however, they still lack the ability to maximize at the same time the amount of PS loaded and the phototoxic effect.

1.9 Degradable Hybrid Nanoparticles to Enhance the PDT Effect

Recently, different groups have explored the possibility of using stimuli-responsive nanoparticles to simultaneously achieve maximum PS loading and high phototoxic effect. These external stimuli can arise from a redox, pH response, be light or enzymatically activated.[65] For example, the second generation PS Pheophorbide A (PheoA) was conjugated with glycol chitosan (GC) polymer via a cleavable disulfide linker. The formulation was able to self-assemble in aqueous conditions to form core-shell NPs (PheoA-ss-CNPs). However, once the PheoA-ss-CNPs are internalized by cancer cells, the disulfide bonds are broken due to the intracellular reducing environment. The reduction of the disulfide bond affords the delivery of PheoA as individual molecules. This platform exhibited increased phototoxicity both *in vitro* and *in vivo* when compared to amide linked PheoA-CNPs. In another approach, PheoA was encapsulated inside human serum albumin (HSA) NPs for PDT. This platform has the ability to be triggered enzymatically and by an acidic environment. The PS was released as individual units once inside the lysosome increasing the overall PDT effect when compared to free PheoA. This is due to the degradability of the HAS nanocarriers.[66,67] Our group has focused on the development of stimuli-responsive hybrid NPs, which are composed of both organic and inorganic components. This platform can be used to design NP-based

degradable systems with high payload of PSs. Under specific conditions inside cancer cells, the hybrid NPs can be degraded to release the PS molecules as individual units to achieve maximum PDT effect. In particular, we have recently developed hybrid redox-responsive polysilsesquioxane nanoparticles (RR-PSilQ NPs) for PDT.[68] Several advantages can be envisioned by using PSilQ NPs for PS delivery such as tunable size, morphology, chemical properties, biodegradability and biocompatibility. The PSilQ platform contains protoporphyrin IX (PpIX) as PS agent. Two building molecules based on PpIX were synthesized in this study, control (C-PpIX) and redox-responsive (RR-PpIX) derivatives (Figure 6). Both compounds include triethoxy silane groups which after condensation in a reverse microemulsion reaction afford the hybrid PSilQ NPs. The RR-PpIX ligand incorporates a disulfide bond that will be cleaved under reducing conditions such as those found inside of cancer cells. The structural properties of these PSilQ-NPs showed that we can synthesize NPs with a size of 50-200 nm in diameter and a high content of PSs on the order of 43-46 (wt%). Moreover, we have shown that once the PSilQ NPs have been internalized in the cells, the redox-responsive PSilQ platform increases photototoxicity in comparison to the control material (Figure 7). The difference observed is due to the degradability of the RR-PpIX system helps to avoid the interactions between the hydrophobic PpIX molecules and increase the amount of $^1O_2$ that can be produced. This effect increases the overall PDT outcome in human cervical cancer cells (HeLa) cells as shown in Figure 7.[68]

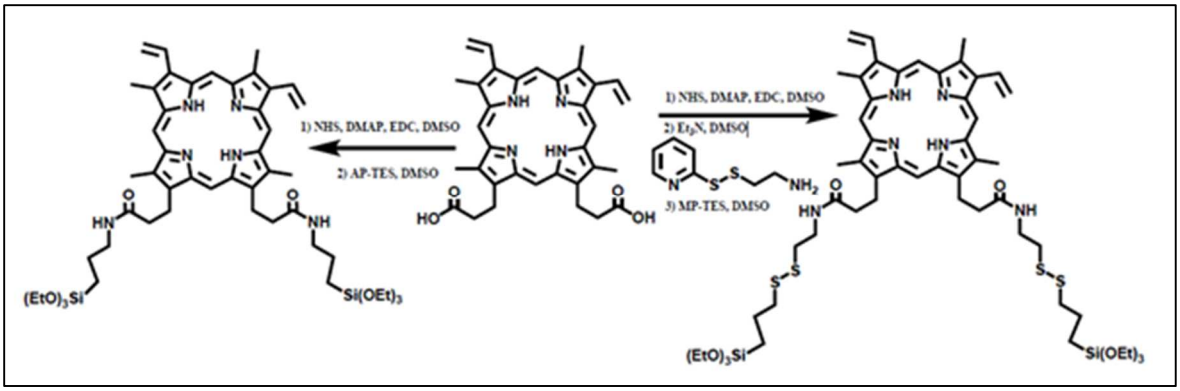

Figure 6: Schematic representation of the synthesis of PpIX-APTES (C-PpIX) (**left**) and PpIX-MPTES (RR-PpIX) (**right**) ligands.

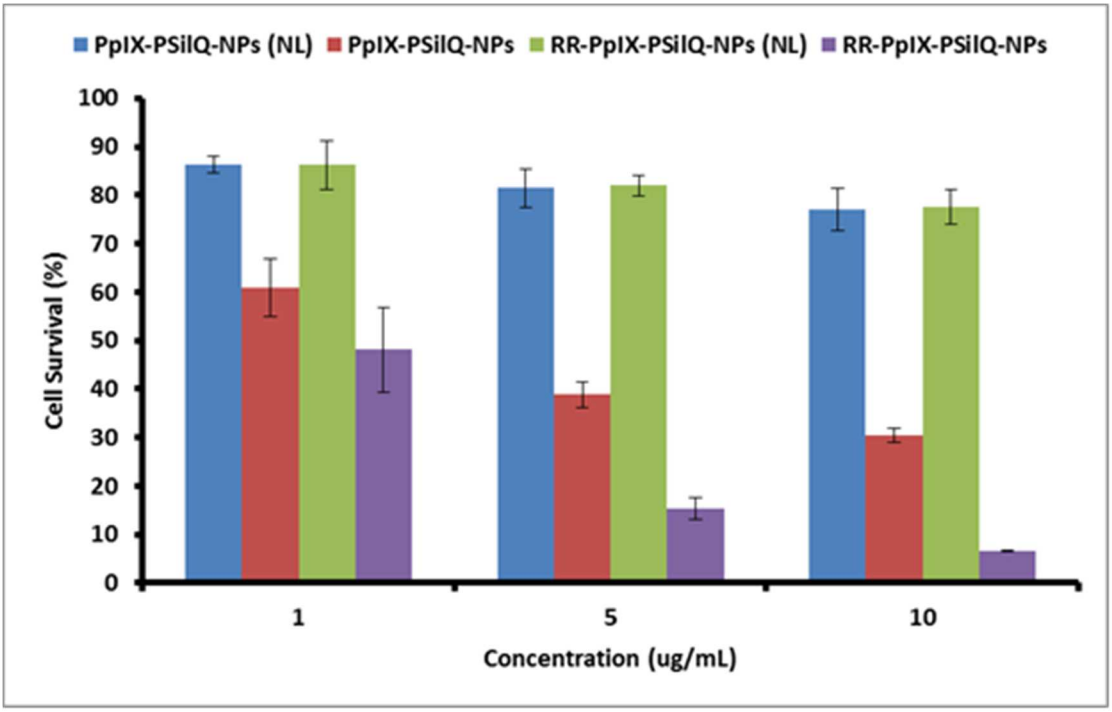

Figure 7: Phototoxicity of PpIX-PSilQ NPs (blue) and RR-PpIX-PSilQ NPs (green) in the absence of light, and PpIX-PSilQ NPs (red) and RR-PpIX-PSilQ NPs (purple) after light exposure (400–700 nm; 170 ± 3 mW cm^{-2}) for 20 min, measured by MTS assay.[68]

To corroborate that PpIX molecules are released from the RR-PpIX-PSilQ platform inside the cancer cells, the PpIX derivatives (C-PpIX and RR-PpIX) were attached to fluorescein isothiocyanate (FITC) labeled SiNPs to observe *in vitro* delivery of PpIX from RR-PpIX-SiNPs. Confocal microscopy images demonstrated that indeed PpIX

molecules are released from the nanoparticles (Figure 8).[44] This PpIX-SiNP system follows the same trend in phototoxicity where the RR-PpIX-SiNPs showed a higher phototoxic effect than the control PpIX-SiNPs. Overall, these results demonstrated that PSilQ nanoparticles can be designed to afford PS delivery platforms with degradable properties and high content of PS molecules. However, this current approach also displayed a high degree of aggregation under physiological conditions with the inability for further modification due to the lack of functional groups. It is critical to resolve the issues associated with the PSilQ platform in order to move it forward for *in vivo* experiments.

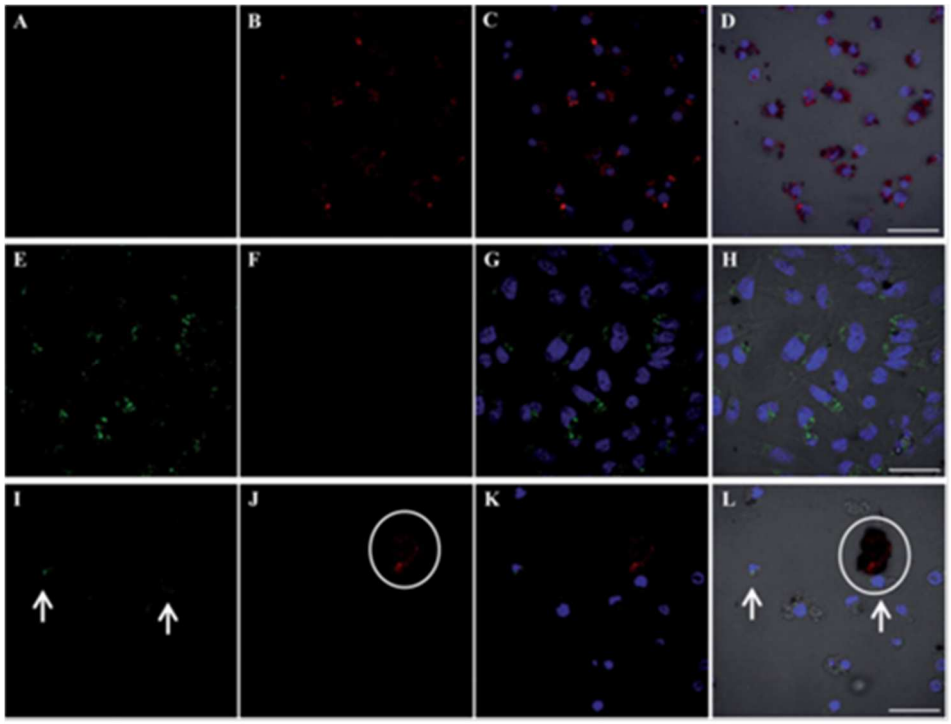

Figure 8: Confocal fluorescence images of HeLa cells inoculated with PpIX in solution (A–D), PpIX–SiNP (E–H), and RR–PpIX–SiNP (I–L). Green fluorescence of the FITC-functionalized nanoparticles (A, E and I); red fluorescence of PpIX molecules (B, F and J); the overlapped image of green, red and DAPI-stained nuclei (C, G and K); and the overlapped image with the DIC channel (D, H and L). Scale bars = 30 μm (A–D & I–L); 20 μm (E–H). The circles show the release of PpIX molecules and the arrows show the presence of the FITC-labeled RR–PpIX–SiNP.[44]

1.10 Research Objective

The main target of this thesis is to develop degradable PSilQ-based nanoparticles with improved colloidal stability and tunable surface properties. The PS molecule for this study is the tetrakis (carboxyphenyl) porphyrin (TCPP) derivative. We hypothesize that the increase in connectivity compared to PpIX will allow the fabrication of monodisperse PSilQ NPs with higher amount of PS molecules. In addition; the designed TCPP monomers contain additional carboxylic acid groups that after the synthesis of the PSilQ nanoparticles can be used for further functionalization with polymers and targeting molecules.

1.10.1 Design and Synthetic Strategy

Two versions of TCPP derivatives were synthesized; the control TCPP (C-TCPP) building block, and the redox-responsive TCPP (RR-TCPP) version that holds a labile disulfide bond (Figure 9). These TCPP molecules contain a triethoxysilane group to afford the corresponding PSilQ NPs after condensation reaction and carboxylic acid groups for further functionalization. The synthesis of PSilQ NPs was carried out by a reverse microemulsion method. The PSilQ NPs were modified with either methoxy-polyethylene glycol amine (MeO-PEG-NH_2) or folic acid-polyethylene glycol amine (FA-PEG-NH_2) chains by coupling chemistry. The functionalization of the PSilQ-NPs with MeO-PEG-NH_2 and FA-PEG-NH_2 polymers will increase their biocompatibility and targeting capabilities. To achieve the steps mentioned above, the following specific aims were pursued in this project: 1) To synthesize and characterize folic acid-polyethylene glycol-amine (FA-PEG-NH_2) and methoxy polyethylene glycol-amine (MeO-PEG-NH_2); 2) To synthesize and characterize the C-TCPP and RR-TCPP silane derivatives and 3) To

synthesize and characterize TCPP-loaded multifunctional PSilQ NPs with target-specific capabilities toward cancer cells.

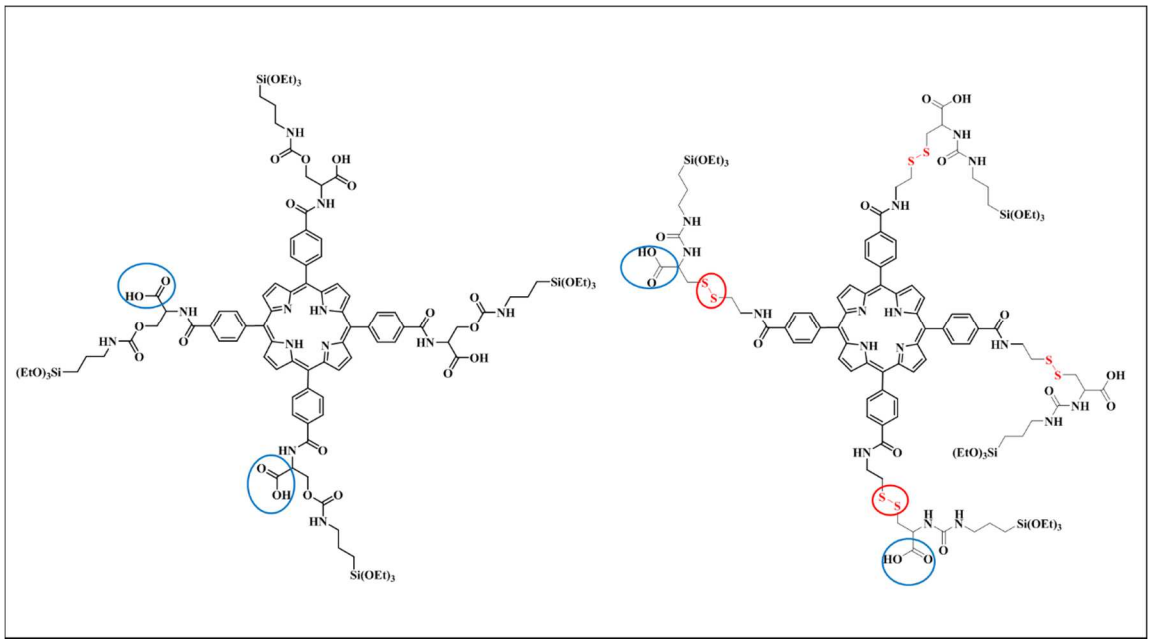

Figure 9: Schematic representation of C-TCPP (**left**) and RR-TCPP (**right**) that will be synthesized to afford biodegradable PSilQ NP (**red** circle indicates redox-responsive properties; **blue** circle indicates amino acid groups for functionalization with FA-PEG-NH_2.)

1.10.2 Synthesis of Folic acid-Polyethylene glycol-Amine (FA-PEG-NH_2) and Methoxy Polyethylene glycol-Amine (MeO-PEG-NH_2)

PEG is an FDA approved polymer that shows good solubility in both organic and aqueous solvents. It is also biocompatible with both blood and tissue and nontoxic to cellular systems.[69] PEG also reduces opsonization and allows for longer circulation times of PEG modified NPs in the body.[70] In this project, PEG derivatives are synthesized and characterized to modify the surface properties of the TCPP-loaded PSilQ NPs. Furthermore, the PEG chain derivatives are also used as linkers to attach targeting agents. There is a wide variety of targeting ligands that can be used to functionalized

nanoparticles such as antibodies, aptamers, peptides and small molecules. In this work, we used a small molecule (folic acid) to target TCPP-loaded PSilQ NPs toward cancer cells. Folic acid is a vitamin that is necessary for normal cells to function properly; however, in the case of cancer cells, folate receptors are overexpressed for this small vitamin due to their rapid proliferation and growth. Folic acid has been widely used as a targeting moiety in the design of anticancer nanoparticles.[71] MeO-PEG-NH_2 and FA-PEG-NH_2 polymer chains were synthesized through a multi-step synthesis (Schemes 1 and 2).

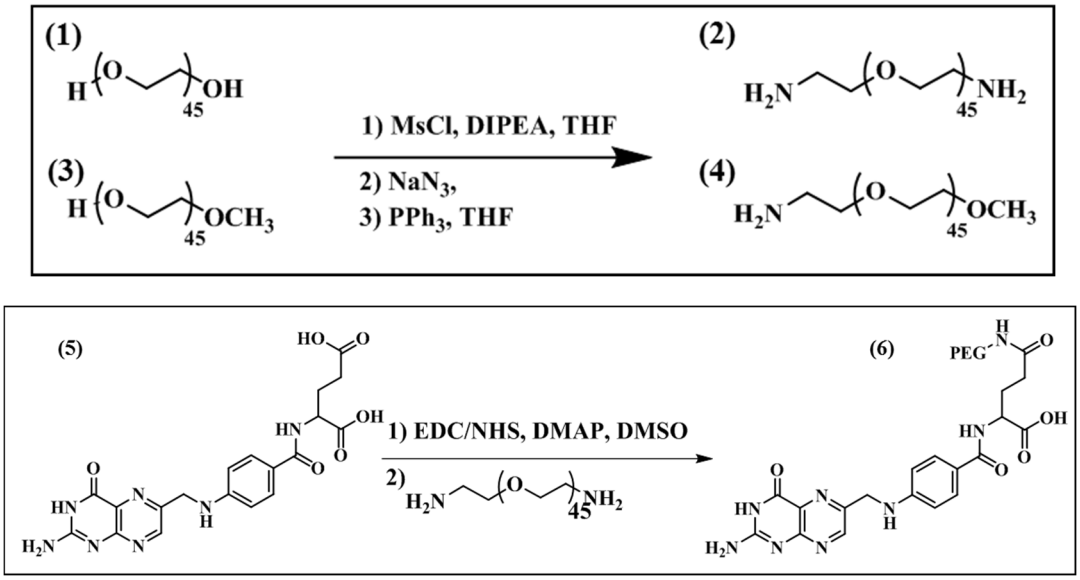

Schemes 1 and 2: Synthesis of MeO-PEG-NH_2 and NH_2-PEG-NH_2 (Scheme 1, top) and of FA-PEG-NH_2 (Scheme 2, bottom) polymers.

1.10.3 Synthesis of C-TCPP and RR-TCPP Silane Derivatives

The synthesis of the TCPP-based building blocks (Figure 9) was carried out following the synthetic steps depicted in (Schemes 3, 4 and 5). C-TCPP and RR-TCPP silane derivatives contain carboxylic and alkoxysilane groups that increased their solubility under basic conditions to afford PSilQ NPs after the polymerization reaction. Furthermore, RR-TCPP silane molecule contains a disulfide bond that is cleaved under

reducing environment such as those found in cancer cells. This allows the release of individual monomeric units of the PS, which limits self-quenching and produces an enhancement in the phototoxic effect.

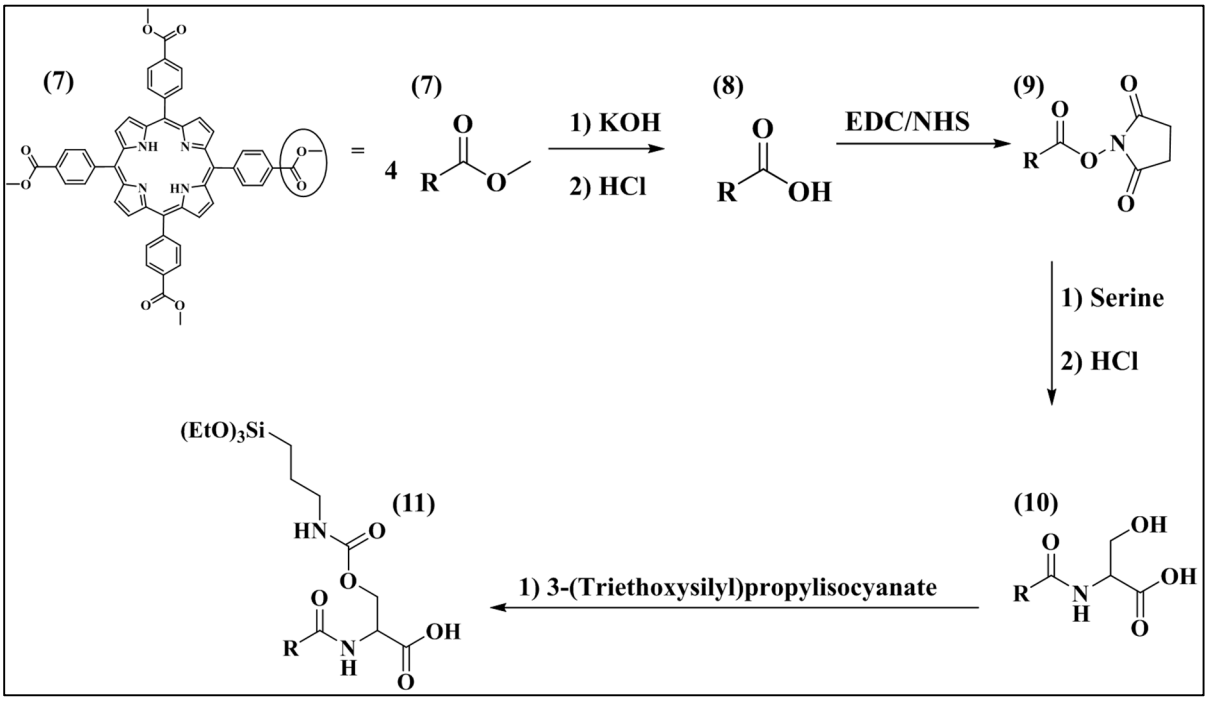

Scheme 3: Synthetic steps to afford the C-TCPP building block.

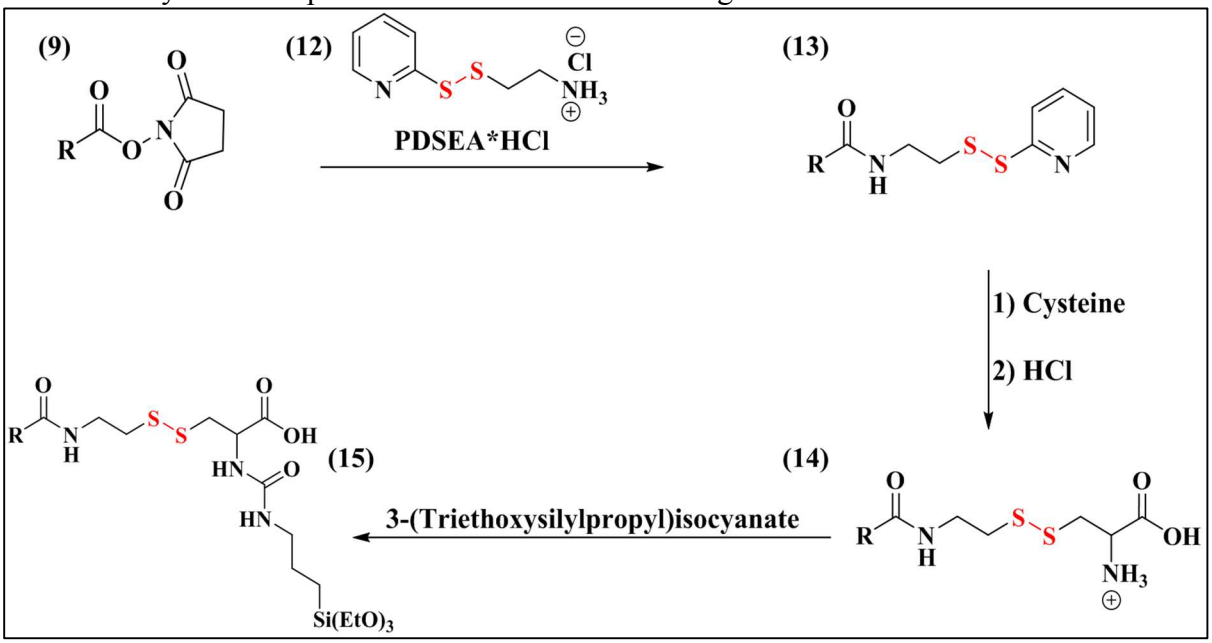

Scheme 4: Synthetic steps to afford the RR-TCPP building block.

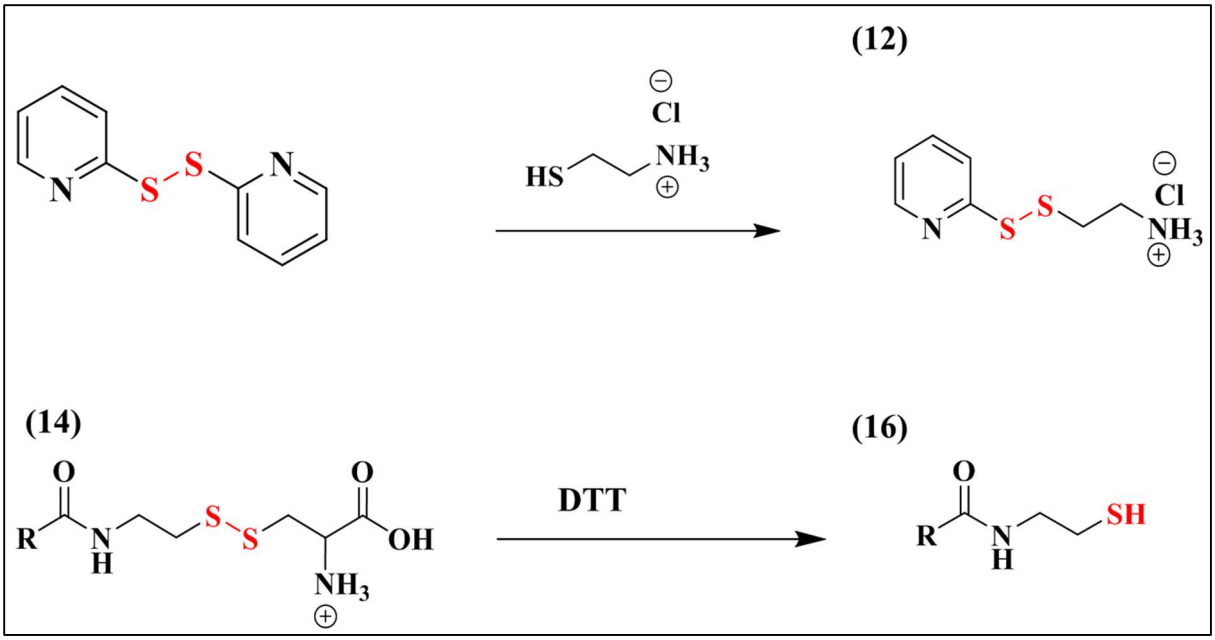

Scheme 5: Synthesis of PDSEA*HCl and reduction of TCPP-Cysteine with DTT to afford TCPP-ethyl thiol.

1.10.4 Synthesis of Target-specific TCPP-loaded PSilQ NPs

PSilQ NPs were synthesized using the reverse microemulsion technique. This process requires a two-phase system comprised of surfactant, co-surfactant, organic solvent, silica precursor, and water. In this system, micellar nanoreactors are formed from an aqueous phase being surrounded by a hydrophobic environment. The size of the NPs can be finely tuned by changing the water to surfactant ratio. This method is optimal for constructing monodispersed NPs smaller than 100 nm.[72] In our project, the C-TCPP and RR-TCPP serve as monomers for the condensation reaction. These silica precursors are the main components of the framework for PSilQ NPs. By using this synthetic strategy we obtained monodisperse PSilQ NPs with a high content of PS molecules (~30% in weight) and sizes below 200 nm in diameter. Moreover, the surface of the nanoparticle is partially covered with carboxylic acid groups, which were used to further functionalize

the NPs with MeO-PEG-NH_2 and FA-PEG-NH_2 polymers to afford target-specific PSilQ-NPs (Figure 10).

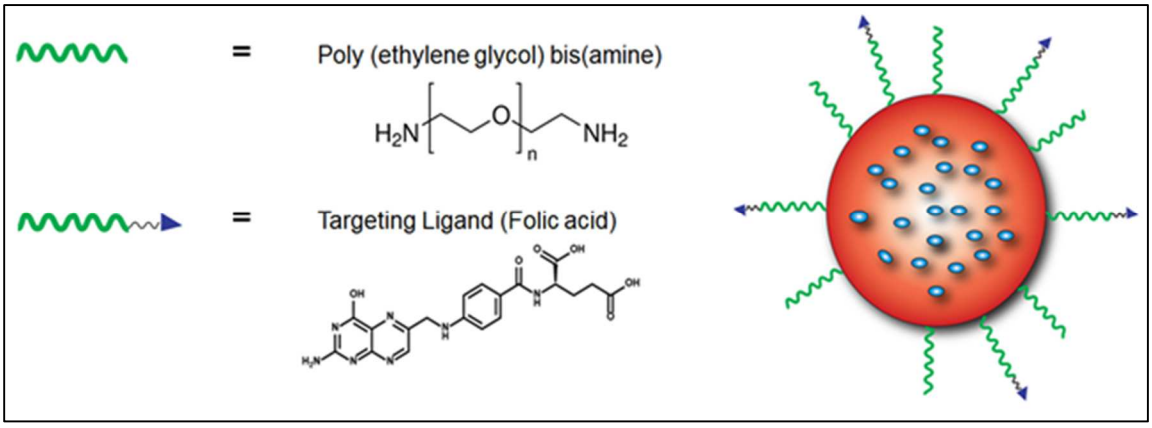

Figure 10: Schematic representation of PEG-FA-TCPP PSilQ NP with a high payload of PS (**green** indicates PEG-FA; **red** indicates the PSilQ NP with the PS (**blue**) as the framework).

CHAPTER 2: EXPERIMENTAL

2.1 Synthesis and characterization of Folic acid-Polyethylene glycol-Amine (FA-PEG-NH_2) and Methoxy Polyethylene glycol-Amine (MeO-PEG-NH_2)

The synthesis of MeO-PEG-NH_2 and FA-PEG-NH_2 was carried out through a multi-step synthetic approach (Scheme 1 and 2) following a procedure reported in the literature with slight modifications.[77-80] Below, the experimental conditions and characterization for each step in the synthesis of both PEG polymer derivatives is described.

2.1.1 Synthesis of Diazido-PEG_{2000} (1)

To synthesize Diazido-PEG_{2000}, 2.0 g of poly(ethylene glycol) (PEG) (1.0 mmol) was dried under vacuum overnight. The following day, the dried-PEG was combined with 1.62 mL of methanesulfonyl chloride (21.0 mmol) in anhydrous tetrahydrofurane (THF) (10.0 mL) at 70 °C. The mixture was then stirred in an ice bath under N_2 atmosphere, followed by the addition of a solution of 3.06 mL of di-isopropylethylamine (DIPEA) (17.6 mmol) in THF (10.0 mL) dropwise over 30 min. Thereafter, the solution was stirred for 1 h followed by removing the reaction flask from the ice bath. The mixture was stirred overnight at room temperature. The newly formed solid was dissolved by the addition of cold H_2O (10.0 mL) on an ice bath. Next, 1.0 N sodium bicarbonate (2.0 mL) and 1.5 g sodium azide (23.1 mmol) were added to the solution. THF was removed from the mixture using rotatory evaporation and the aqueous phase was refluxed at 100 °C for 24 h with stirring. The product was obtained after extraction with dichloromethane (DCM) (5 x 15.0 mL) followed by washing steps with brine (5 x

15.0 mL) and removal of the excess water in the presence of magnesium sulfate. DCM was removed by rotary evaporation to afford the final product, Diazido-PEG_{2000}, as a white solid compound (2.1 g, 84%). The product was dried under high vacuum and stored at -20 °C. The diazido-PEG_{2000} polymer was confirmed by the stretching vibration of the azido group in IR (2110 cm^{-1}). The shift of methylene protons suggests a successful synthesis of PEG-N_3 from PEG. The ethylene carbons also show a shift from the starting material, PEG. IR: (1102 cm^{-1} (C-O), 2110 cm^{-1} (azide); ^{1}HNMR: (300 MHz; $CDCl_3$): δ_H, ppm- (t, 4H, 3.32-3.42), (m, 168H, 3.54-3.76).

2.1.2 Synthesis of Diamino-PEG_{2000} (2)

To synthesize diamino-PEG_{2000}, 1.36 g of diazido-PEG_{2000} (680 μmol) was combined with 2.1 g triphenylphosphine (8 mmol) in anhydrous THF (10.0 mL). This solution was stirred under N_2 atmosphere at room temperature overnight. After that, H_2O (510 μL) was added and the mixture was again stirred overnight. THF was removed by rotary evaporation and water (17.0 mL) was added. A white solid was formed (triphenyl phosphinoxide) immediately after the addition of H_2O. The solid and H_2O were removed by gravity filtration and rotary evaporation, respectively. Finally, a yellowish solid (1.3 g, 98%) corresponding to diamino-PEG_{2000} was dried under high vacuum and stored at -20 °C. The diamino-PEG product was confirmed by the disappearance of the stretching vibration for the azido group in the IR and the chemical shift of methylene protons close to the amine groups at 2.91-2.97 ppm. IR: 1102 cm^{-1} (C-O); ^{1}HNMR: (300 MHz; d_4-Methanol): δ_H, ppm- (t, 4H, 2.91-2.97), (m, 168H, 3.54-3.76).

2.1.3 Synthesis of Azido-methoxy-PEG_{2000} (3)

To synthesize azido-methoxy-PEG_{2000}, 2.0 g poly(ethylene glycol) methyl ether ($mPEG_{2000}$) (1.0 mmol) was combined with 1.5 mL methanesulfonyl chloride (19.4 mmol) in anhydrous THF (10.0 mL). The mixture was stirred in an ice bath under N_2 atmosphere, followed by the addition of a solution of 3.0 mL DIPEA (17.2 mmol) in THF (10.0 mL) dropwise over 30 min. After that, the solution was stirred for 1 h followed by removing the reaction flask from the ice bath. The mixture was stirred overnight at room temperature. The newly formed solid was dissolved by the addition of cold water (10.0 mL) on an ice bath. Next, 1.0 N sodium bicarbonate (2 mL) and 1.5 g sodium azide (23.1 mmol) were added to the solution. Next, THF was removed from the mixture using rotatory evaporation and the aqueous phase was refluxed at 100 °C for 24 hr. The product was obtained after extraction with dichloromethane (DCM) (5 x 15.0 mL) followed by washing steps with brine (5 x 15.0 mL) and removal of the excess water in the presence of magnesium sulfate. DCM was removed by rotary evaporation to afford the final product, azido-methoxy-PEG_{2000}, as a white solid compound (1.6 g, 76%). The product was dried under high vacuum and stored at -20 °C. The azido-methoxy-PEG2000 polymer was confirmed by the stretching vibration of the azido group in IR (2110 cm^{-1}). Moreover, the methylene protons show a shift from the starting mPEG material. IR: 2110 cm^{-1} (azide); ^{1}HNMR: (300 MHz; $CDCl_4$): δ_H, ppm- (m, 7H, 3.33-3.41), (m, 168H, 3.57-3.76).

2.1.4 Synthesis of amino-methoxy-PEG_{2000} (4)

To synthesize amino-methoxy-PEG_{2000}, 1.8 g of azido-methoxy-PEG_{2000} (900 µmol) was combined with 1.5 g of triphenylphosphine (5.7 mmol)) in anhydrous THF (12.0 mL). This solution was stirred under N_2 atmosphere at room temperature

overnight. After that, water (1.4 mL) was added and the mixture was again stirred overnight. THF was removed by rotary evaporation and water (21.0 mL) was added. Immediately after the addition of water a white solid (triphenyl phosphinoxide) was formed. The solid and water were removed by gravity filtration and rotary evaporation, respectively. Finally, a yellowish solid (1.0 g, 56%) corresponding to amino-methoxy-PEG_{2000} was dried under high vacuum and stored at -20 °C. The amino-methoxy-PEG product was confirmed by the disappearance of the stretching vibration for the azido group in the IR and the chemical shift of methylene close to the amine groups at 2.85-2.96 ppm. IR: 1102 cm^{-1} (C-O); ^{1}HNMR: (300 MHz; $CDCl_4$): δ_H, ppm- (t, 4H, 2.85-2.96), (s, 3H, 3.32-3.42), (m, 168H, 3.48-3.82).

2.1.5 Synthesis of succinimide ester of Folic acid (FA-SE) (5)

To synthesize FA-SE, 1.5 g of FA (3.4 mmol) was combined with 978 mg of N-hydroxysuccinamide (NHS) (8.5 mmol), 622 mg of 4-(dimethylamino) pyridine (DMAP) (5.1 mmol) and 1.3 g of N-(3-dimethylaminopropyl)-N'-ethylcarbodiimide hydrochloride (EDC) (6.8 mmol) in anhydrous dimethylsulfoxide (DMSO) (50.0 mL). The solution was stirred for 48 h at room temperature. The succinimide ester derivative was dried using a lyophilizer. The final product, a yellow solid was stored at -20 °C. The partial esterification of FA was confirmed by the appearance of the succinimide group in the IR. The appearance of the ethylene protons in the ^{1}H NMR provide evidence for the presence of SE. IR: 1688 cm^{-1} (FA), 1718 cm^{-1}(ester), 1782 cm^{-1}(NHS), 1820 cm^{-1}(NHS); ^{1}HNMR: (300 MHz, d_6-DMSO): δ_H, ppm-(m, 2 H, 1.85-2.12), (t, 2 H, 2.28-2.34) (s broad, 4 H, 2.79), (m, 1 H, 4.31-4.35), (d, 2 H, 4.47-4.49), (d, 2 H, 6.62-6.65), (t, 1H, 6.92-6.96), (d, 2 H, 7.63-7.66), (d, 1 H, 8.12-8.14), (s broad, 1 H, 8.65).

2.1.6 Synthesis of Folic acid amino-PEG_{2000} (6)

To synthesize folic acid amino-PEG_{2000}, 432 mg of diamino-PEG_{2000} (216 μmol) was combined with 175 mg FA-SE (325 μmol) in DMSO (20.0 mL). The mixture was stirred for 48 h at room temperature. The material was purified by dialysis with water for 7 days changing the water twice per day. (Slide-A-Lyzer® dialysis cassette, MWCO 2000). The dialyzed solution was dried using a lyophilizer. The final product, a yellow solid, was stored at -20 °C. The product was confirmed by the appearance of an amide bond in the IR when compared to the starting FA material. A mono-substituted product is desired in order to effectively attach the targeting moiety to the PSQ NPs. The target compound was purified using dialysis and the mono-substitution was visualized using ^{1}H NMR. The integration for the polymer, PEG and the FA protons suggests a mono-substituted product was obtained after dialysis**.** (Yield: 105 mg, 20%); IR: 1101 cm^{-1}(C-O), 1644 cm^{-1} (amide) 1686 cm^{-1}(FA); ^{1}HNMR: (300 MHz, d_6-DMSO): δ_H, ppm-(m, 2 H, 1.85-2.12), (t, 2 H, 2.28-2.34), (m, 90 H, 3.54-3.78), (m, 1 H, 4.31-4.35), (d, 2 H, 4.47-4.49), (d, 2 H, 6.62-6.65), (t, 1H, 6.92-6.96), (d, 2 H, 7.63-7.66), (d, 1 H, 8.12-8.14), (s broad, 1 H, 8.65); ^{13}CNMR: (500 MHz; D_2O): δ_C- 28.56, 32.74, 34.40, 39.10, 45.81, 51.99, 69.36, 112.55, 121.90, 127.58, 129.10, 148.81, 150.82, 156.00, 162.00, 169.66, 175.71

2.2 Synthesis and characterization of control tetrakis(carboxy)phenyl porphyrin (C-TCPP) and redox-responsive tetrakis(carboxy)phenyl porphyrin (RR-TCPP) silane derivatives

The synthesis of the novel C-TCPP and RR-TCPP building blocks was carried out through a multi-step synthetic approach (Schemes 3, 4 and 5). Below, the experimental

conditions and characterization for each step in the synthesis of both molecules is described.

2.2.1 Synthesis of 5,10,15,20-Tetrakis(carbomethoxy)phenyl porphyrin (TCM_4PP) (7)

To synthesize TCM_4PP, 2.294 g of methyl-4-formyl benzoate (14.0 mmol) was added to propionic acid (150.0 mL) with stirring and heated to 151 °C. Then, 970 µL (14.0 mmol) of pyrrole was added and the solution was allowed to reflux for 1 h. The product was purified by washing with cold methanol and filtered. The deep purple crystals were dried under high vacuum and stored at room temperature. (Yield: 651 mg, 22.0%). The successful synthesis of TCM_4PP was confirmed by the appearance of an ester peak in the IR (1720 cm^{-1}). The protons for the porphyrin, the phenyl and the methyl ester were observed in the ^1H NMR (8.8, 8.4, 8.3 and 4.1 ppm). The aliphatic carbons for the methyl ester are observed in the ^{13}C NMR (52.60 ppm). The positive ion is visualized in the MALDI ($[M+1]^+$ = 847.34). A calibration curve in DMF of this compound was obtained by UV-vis spectrometry. The extinction coefficient calculated was 361,700 M^{-1} cm^{-1}(λ = 419 nm). IR: 1720 cm^{-1}; ^{1}HNMR: (300 MHz; $CDCl_3$): δ_H, ppm- (s, 12 H, 4.1), (d, 8 H, 8.3), (d, 8 H, 8.4), (s, 8 H, 8.8); ^{13}CNMR: (300 MHz; $CDCl_3$): δ_C, ppm- 52.60, 119.51, 128.11, 129.87, 131.21, 134.64, 146.72, 167.35(ester); Calculated mass for **TCM_4PP**: $C_{52}H_{36}N_4O_8$, 846.90 g/mol; MS (MALDI positive ion): m/Z 847.34 $[M+1]^+$, 848.67 $[M+2]^+$, 849.38 $[M+3]^+$; Absorbance (DMF): Soret band (λ_{max} = 419 nm, ε = 361,700 M^{-1} cm^{-1}, r^2 = 0.9972).

2.2.2 Synthesis of Tetrakis(carboxy)phenyl porphyrin (TCPP) (8)

To synthesize TCPP, 500 mg of TCM_4PP (590 µmol) was added to a mixture of THF:EtOH (30 mL; 1:1 vol.) containing 4 mL of KOH (2 M). The mixture was stirred at

70 °C for 24 h. The product was obtained by evaporating the solvent mixture and dissolving in 300 mL of water followed by the addition of 850 µL HCl (37%/v) to allow precipitation. The dark blue crystals were filtered, dried under high vacuum and stored at room temperature. (Yield: 452 mg, 96.8%). The successful synthesis of TCPP was confirmed by a shift in IR from methyl ester to acid (1694 cm^{-1}). The disappearance of the methoxy group in the ^{1}H NMR and ^{13}C NMR was evidence for the synthesis of TCPP. The parent ion for TCPP was observed in the MALDI ([M] = 790.0). A calibration curve in DMF of this compound was obtained by UV-vis spectrometry. The extinction coefficient calculated was 399,000 M^{-1} cm^{-1} (λ = 419 nm). IR: 1694 cm^{-1}; ^{1}HNMR: (300 MHz, d_6-DMSO): δ_H, ppm- (q, 16 H, 8.26-8.39), (s, 8 H, 8.85); ^{13}CNMR: (500 MHz, d_6-DMSO): δ_C, ppm- 119.84, 128.43, 129.95, 131.00, 132.16, 134.99, 145.95 167.97(acid); Calculated mass for **TCPP**: $C_{48}H_{28}N_4O_8$, 790.79 g/mol; MS (MALDI): m/Z [M], 790.0; Absorbance (DMF): Soret band (λ_{max} = 419 nm, ε = 399,000 M^{-1} cm^{-1}, r^2 = 0.9989).

2.2.3 Synthesis of succinimide ester of TCPP (TCPP-SE) (9)

To synthesize TCPP-SE, 455 mg of TCPP (575 µmol) was combined with 993 mg NHS (8.6 mmol), 422 mg DMAP (3.5 mmol) and 1.1 g EDC (5.7 mmol) in a mixture of DCM:DMSO (110 mL; 1.75:1 vol.). This solution was stirred for 2 h in an ice bath. After that, the mixture was removed from the ice bath and stirred for another 48 h at room temperature. The succinimide ester derivative was purified by precipitation in aqueous solution containing 20% EtOH. The magenta colored solid was washed several times with the same solution and dried using a lyophilizer. The final product was stored at -20 °C (Yield: 651 mg, 96%).The successful synthesis of TCPP-SE was confirmed by

the appearance of the ester and succinimide groups in the IR (1736, 1770 and 1803 cm^{-1}). The appearance of the ethylene protons in the ^{1}H NMR and aliphatic carbons in the ^{13}C NMR suggest an attachment of the SE (3.00 and 26.15 ppm). The positive ion was observed in the MALDI for TCPP-SE ($[M+1]^{+}$ = 1176.04). A calibration curve in DMF of this compound was obtained by UV-vis spectrometry. The extinction coefficient calculated was 295,100 M^{-1} cm^{-1} (λ = 419 nm). IR: 1736 cm^{-1}(ester), 1770 cm^{-1}(NHS), 1803 cm^{-1}(NHS); ^{1}HNMR: (300 MHz, d_6-DMSO): δ_H, ppm-(s broad, 16 H, 3.00), (q, 16 H, 8.51-8.58), (s, 8 H, 8.95); ^{13}CNMR: (500 MHz, d_6-DMSO): δ_C, ppm-26.15(methylene), 162.64(ester), 171.01(NHS). Calculated mass for **TCPP-SE**: $C_{68}H_{46}N_4O_{16}$, 1175.13 g/mol; MS (MALDI positive ion): m/Z 1176.04 $[M+1]^{+}$, 1177.42 $[M+2]^{+}$, 1178.56 $[M+3]^{+}$; Absorbance (DMF): Soret band (λ_{max} = 420 nm, ε = 295,100 M^{-1} cm^{-1}, r^2 = 0.9953).

2.2.4 Synthesis of TCPP serine derivative (TCPP-Serine) (10)

To synthesize TCPP-Serine, 300 mg of TCPP-SE (255 µmol) was combined with 203 mg of L-serine hydrochloride (1.9 mmol) and 437 µL N,N-Diisopropylethylamine (DIPEA) (2.5 mmol) in DMSO (25 mL). The serine was first dissolved in water (3.75 mL) before adding to DMSO. The mixture was stirred for 48 h at 100 °C. After that, the serine derivative was purified by precipitation in aqueous solution containing 25% EtOH followed by the addition of 180 µL HCl (37%/v). The blue crystals were washed several times with the same solution and dried using a lyophilizer. The final product was stored at -20 °C (Yield: 243 mg, 84%). The successful synthesis of TCPP-Serine was confirmed by the disappearance of the ester and succinimde groups. A new peak in the IR was evidence for the formation of an amide bond (1634 cm^{-1}). The appearance of the protons

and carbons for the amino acid serine, suggests a successful conversion (3.92, 4.63, 56.41 and 61.86 ppm). The parent ion for the TCPP-Serine was also observed ($[M+1]^+$ = 1138.70). A calibration curve in DMF of this compound was obtained by UV-vis spectrometry. The extinction coefficient calculated was 324,600 M^{-1} cm^{-1} (λ = 419 nm). IR: 1634 cm^{-1} (amide); ^{1}HNMR: (300 MHz; d_6-DMSO): δ_H, ppm- (d, 8H, 3.92-3.94), (m, 4H, 4.63-4.69); ^{13}CNMR: (300 MHz; d_6-DMSO): δ= 56.41, 61.86 (aliphatic carbons), 166.93(amide), 172. 57(acid); Calculate mass for **TCPP-Serine**: $C_{60}H_{50}N_8O_{16}$, 1139.10 g/mol; MS (MALDI): m/Z [M] 1138.70; Absorbance (DMF): Soret band (λ_{max} = 419 nm, ε = 324,600 M^{-1} cm^{-1}, r^2 = 0.9994).

2.2.5 Synthesis of control TCPP silane derivative (C-TCPP) (11)

To synthesize C-TCPP, 170 mg of TCPP-Serine (149 µmol) was combined with 155 µL of 3-(triethoxysilyl)propyl isocyante (TES-PI) (626 µmol) and 183 µL triethylamine (Et_3N) in anhydrous N,N-Dimethylformamide (DMF) (10 mL) and stirred for 2 h in an ice bath under N_2 atmosphere. The mixture was removed from the ice bath and stirred at room temperature for another 20 h under N_2 atmosphere. The control ligand was obtained by precipitation in 80 mL of water followed by the addition of 150 µL of HCl (37%/v). The black powder was washed several times with the same solution and dried using a lyophilizer. The final product was stored at -20 °C (Yield 219 mg, 69%): The successful synthesis of C-TCPP was confirmed by an appearance of the peaks for a carbamate carbonyl, silicon-carbon and silicon-oxygen in the IR (1016, 1233 and 1706 cm^{-1}). NMR was difficult to obtain due to the poor solubility of the compound. A calibration curve in DMF of this compound was obtained by UV-vis spectrometry. The extinction coefficient calculated was 271,400 M^{-1} cm^{-1}(λ = 415 nm). IR: 1016 cm^{-1} (Si-

O), 1233 cm^{-1} (Si-C), 1706 cm^{-1} (carbamate); Absorbance (DMF): Soret band (λ_{max} = 415 nm, ε = 271,400 M^{-1} cm^{-1}, r^2 = 0.9613).

2.2.6 Synthesis of 2-(pyridine-2yl-disulfanyl) ethanamide hydrochloride (PDSEA*HCl) (12)

To synthesize PDSEA*HCl, cysteamine hydrochloride (1.132 g, 9.96 mmol) was dissolved in MeOH (10mL) and added dropwise to a mixture of 2,2'-dipyridyl disulfide (4.4062 g, 20 mmol) and acetic acid (800 µL, 99%/v) in MeOH (20 mL) over 30 min. The mixture was stirred at room temperature for 24 h. The compound was purified by rotatory evaporation of MeOH followed by precipitation with diethyl ether. The white crystals were dried under high vacuum and stored at room temperature. (Yield: 1.86 g, 84%); IR: 1608 cm^{-1} (aromatic); ^{1}HNMR: (300 MHz; d_6-DMSO): δ_H, ppm- (m, 4H, 2.98-3.18), (t, 1H, 7.27-7.33), (d, 1H, 7.73-7.78), (t, 1H, 7.81-7.88), (s, 3H, 8.16-8.28), (d, 1H, 8.49-8.53); ^{13}CNMR: (300 MHz; d_6-DMSO): δ_C, ppm- 35.30, 38.21 (aliphatic carbons), 120.60, 122.21, 138.49, 150. 40, 158.59 (aromatic carbons).

2.2.7 Synthesis of pyridine disulfide ethylamine of TCPP (TCPP-PDSEA) (13)

To synthesize TCPP-PDSEA, TCPP-SE (314 mg, 267 mmol) was combined with PDSEA*HCl (386 mg, 1.7 mol) and Et_3N (292 µL, 2.1 mmol) in DMSO (6.5 mL) and stirred at 80 °C for 3 days. The product was purified by precipitation in aqueous solution containing 20% EtOH. The brown powder was washed several times with the same solution and dried using a lyophilizer. The final product was stored at -20 °C. (Yield: 195 mg, 50%). The successful synthesis of TCPP-PDSEA was confirmed by the appearance of the aromatic protons in the ^{1}HNMR (7.24, 7.58, 7.76 and 846 ppm). The disappearance of the succinimide groups in IR with an appearance of a peak for an amide bond suggests

a succesful synthesis (1638 cm^{-1}). ^{13}C NMR and MALDI-MS were not obtained for this compound due to its poor solubility. IR: 1605 cm^{-1} (aromatic), 1638 cm^{-1} (amide); $^{1}HNMR$: (300 MHz; d_6-DMSO): δ_H, ppm- (t, 8H, 2.91-3.21), (m, 8H, 3.62-3.89), (t, 4H, 7.24-7.32), (d, 4H, 7.58-7.65), (t, 4H, 7.76-7.85), (q, 16H, 8.16-8.39), (d, 4H, 8.46-8.50), (s, 8H, 9.09).

2.2.8 Synthesis of TCPP-ethyl thiol (TCPP-EtSH) by reduction of TCPP-PDSEA with DL-Dithiothreitol (DTT) (16)

To synthesize TCPP-EtSH, TCPP-PDSEA (66.9 mg, 46 μmol) was combined with DTT (127 mg, 823 μmol) in DMF (6.5 mL). The solution was stirred at room temperature for 24 h. The thiol derivative was purified by precipitation in aqueous solution containing 25% EtOH followed by the addition HCl (60 μL, 37%/v). The brown solid was washed several times with the same solution and dried using a lyophilizer. The final product was stored at -20 °C. (Yield: 31.5 mg, 67%). The successful synthesis of TCPP-EtSH was confirmed by a disapearance of the aromatic protons for the pyridine in the $^{1}HNMR$. ^{13}C NMR and MALDI-MS were not obtained for this compound due to its poor solubility. $^{1}HNMR$: (300 MHz; d_6-DMSO): δ_H, ppm- (q, 8H, 2.74-2.85), (m, 8H, 3.54-3.65), (m, 16H, 8.21-8.42), (s, 8H, 8.86).

2.2.9 Synthesis of cysteine disulfide of TCPP (TCPP-Cysteine) (14)

To synthesize TCPP-Cysteine, TCPP-PDSEA (152 mg, 104 μmol) was combined with L-Cysteine hydrochloride (128 mg, 729 μmol) in DMF (5.2 mL). The solution was stirred at 60 °C for 48 h. The cysteine derivative was purified by precipitation in aqueous solution containing 25% EtOH followed by the addition HCl (180 μL, 37%/v). The reddish-brown material was washed several times with the same solution and dried using

a lyophilizer. The final product was stored at -20 °C. (Yield: 124 mg, 80%). The successful synthesis of TCPP-Cysteine was confirmed by a disapearance of the aromatic protons for the pyridine in the ^{1}HNMR. An appearance of the protons and carbons for the amino acid cysteine, suggests a successful conversion (3.68, 4.28 and 4.63 ppm). ^{13}C NMR and MALDI-MS were not obtained for this compound due to its poor solubility. ^{1}HNMR: (300 MHz; d_6-DMSO): δ_H, ppm- (m, 8H, 2.98-3.11), (m, 8H, 3.52-3.61), (m, 8H, 3.68-3.87), (m, 2H, 4.28-4.41), (m, 2H, 4.63-4.71), (m, 16H, 8.12-8.41), (s, 8H, 8.86).

2.2.10 Synthesis of redox-responsive TCPP silane derivative (RR-TCPP) (15)

To synthesize RR-TCPP, TCPP-Cysteine (153 mg, 61 μmol) was combined with TES-PI (106 μL, 428 μmol) and Et_3N (125 μL, 895 μmol) in anhydrous DMF (11 mL). The solution was stirred in an ice bath for 2 h under N_2 conditions. The mixture was removed from the ice bath and stirred at room temperature for another 20 h still under N_2 atmosphere. The redox-responsive ligand was purified by precipitation in H_2O (60 mL) followed by the addition HCl (150 μL, 37%/v). The black powder was washed several times with the same solution and dried using a lyophilizer. The final product was stored at -20 °C. (Yield: 152 mg, 65%). The successful synthesis of RR-TCPP was confirmed by an appearance of the peaks for carbamide carbonyl, silicon-carbon and silicon-oxygen in the IR. NMR is difficult to obtain due to the poor solubility of the compound. IR: 1019 cm^{-1} (Si-O), 1232 cm^{-1} (Si-C), 1714 cm^{-1} (carbamide).

2.2.11 Singlet Oxygen ($^{1}O_2$) for TCPP, TCPP-Serine and TCPP-EtSH

To measure the amount of $^{1}O_2$ generated by some of the TCPP derivatives, 1,3-diphenylisobenzofuran (DPBF) was used as a $^{1}O_2$ probe. DPBF absorbs at 419 nm in

DMF; however, after the reaction with $^1O_2$, the absorbance at this wavelength decreases. The reduction in DPBF absorbance is proportional to the amount of $^1O_2$ generated. The experimental protocol to measure $^1O_2$ in this work was: DPBF (40 μL, 8 mM) was dissolved with the photosensitizer (10 μL, 2.5 μM) in DMF (4 mL). The solution was irradiated with white light (400-700 nm, 41 mW/cm^2) at different times (20, 40 and 60 s). The absorbance at 419 nm of these solutions was measured using a UV-vis spectrophotometer after illumination. Moreover, control experiments were run in the absence of light. In addition, experiments were carried out using red light (630 -700 nm, 89 mW/cm^2). All the experiments were run by triplicate. The decrease from the original amount of DPBF was used to calculate the $^1O_2$ produced.

2.3 Synthesis and characterization of TCPP-loaded multifunctional PSilQ NPs with target-specific capabilities toward cancer cells

2.3.1 Synthesis of C-TCPP Polysilsesquioxane (PSilQ) NPs (C-TCPP PSilQ NPs)

The synthesis of PSilQ NPs was carried out through a reverse-microemulsion method. Cyclohexane (7.5 mL) was mixed with 1-hexanol (1.6 mL) and Trition X-100 (1.9 mL) and stirred at room temperature for 24 h. In a scintillation vial, a solution of C-TCPP (8 mg) in H_2O (4 mL) and NH_4OH (4 mL) was prepared and immediately added to organic phase solution dropwise. The mixture was allowed to stir at room temperature for 24 h. After that, the C-TCPP PSilQ NPs were obtained by crashing down the material after addition of EtOH (40 mL). The material was separated from the solution by centrifugation. PSilQ particles were washed twice with EtOH to get rid of organic solvent and surfactant. The material was characterized using dynamic light scattering (DLS), ζ-potential, scanning electron microscopy (SEM) and thermogravimetric analysis (TGA).

2.3.2 Synthesis of RR-TCPP Polysilsesquioxane (PSilQ) NPs (RR-TCPP PSilQ NPs)

The synthesis of PSilQ NPs was carried out through a reverse-microemulsion method. Cyclohexane (7.5 mL) was mixed with 1-hexanol (1.6 mL) and Trition X-100 (1.9 mL) and stirred at room temperature for 24 h. In a scintillation vial, a solution of RR-TCPP (8 mg) in H_2O (4 mL) and NH_4OH (4 mL) was prepared and immediately added to organic phase solution dropwise. The mixture was allowed to stir at room temperature for 24 h. Following, the RR-TCPP PSilQ NPs were obtained by crashing down the material after addition of EtOH (40 mL). The material was separated from the solution by centrifugation. PSilQ particles were washed twice with EtOH to remove organic solvent and surfactant. The material was characterized using DLS, ζ-potential, SEM and TGA.

2.3.3 Conjugation of FA-PEG-NH_2 to C-TCPP and RR-TCPP PSilQ NPs

To conjugate FA-PEG-NH_2 polymer to the PSilQ NPs, C-TCPP or RR-TCPP PSilQ NPs (7 mg) was combined with EDC (35 mg) and H_2N-mPEG/FA-PEG-NH_2 (70/30 wt/wt) in anhydrous acetonitrile (10 mL). The mixture was allowed to stir at room temperature under N_2 atmosphere for 48 h. The FA-PEG-NH_2 PSilQ NPs were obtained by evaporating the solvent and re-dispersing in EtOH. The material was characterized using DLS, ζ-potential, SEM and TGA.

2.3.4 Conjugation of H_2N-mPEG to C-TCPP and RR-TCPP PSilQ NPs

To conjugate H_2N-mPEG polymer to PSilQ NPs, C-TCPP or RR-TCPP PSilQ NPs (7 mg) was combined with EDC (35 mg) and H_2N-mPEG (70 mg) in anhydrous acetonitrile (10 mL). The mixture was allowed to stir at room temperature under N_2 atmosphere for 48 h. The H_2N-mPEG PSilQ NPs were obtained by evaporating the

solvent and re-dispersing in EtOH. The material was characterized using DLS, ζ-potential, SEM and TGA.

CHAPTER 3: RESULTS AND DISCUSSION

3.1. Synthesis and characterization of Folic acid-Polyethylene glycol-Amine (FA-PEG-NH_2) and Methoxy Polyethylene glycol-Amine (MeO-PEG-NH_2)

PEG is widely used for drug delivery applications to hinder nanoparticles from the mononuclear phagocyte system.[70] In this work, two versions of PEG derivatives were synthesized to functionalize the TCPP-PSilQ nanoparticles. MeO-PEG-NH_2 polymer enhances the colloidal stability in physiological conditions and neutralizes the charge on the surface of the PSilQ nanoparticles. This molecule is chemically attached to the PSilQ nanoparticles by a conjugation reaction between the amine group in the PEG chain and the carboxylic acid groups chemically available in the PSilQ nanoparticle (Figure 10). In a similar way, FA-PEG-NH_2 polymer contains an amine group to modify the exterior surface of PSilQ NPs. Moreover, this polymer molecule also contains folic acid, which is a well-known targeting agent. FA targets folate receptors that are widely overexpressed in different types of cancer cells. To synthesize the desired MeO-PEG-NH_2 and FA-PEG-NH_2 polymers, a synthetic approach already reported in the literature was followed with slight modifications.[77-80] To convert the alcohol group(s) in the starting materials to amine group(s) (Scheme 1), the polymer was reacted with MsCl in anhydrous THF to afford a good leaving group. The PEG mesylate derivative was reacted with NaN_3, a strong nucleophile, to afford the azido PEG product. The characterization results of the product by ^1H NMR and IR, which are similar to those reported in the literature, strongly suggest the successful synthesis of the desired azide PEG polymer. To convert the azide

derivatives to amines a mild reduction was carried out by following the Staudinger reaction conditions. The azide PEG chain was reacted with $P(Ph)_3$ in anhydrous THF to generate the corresponding iminophosphorane. An aqueous work-up lead to the desired amino PEG derivatives and the very stable phosphine oxide as by-product. The characterization data by IR showed the disappearance of the stretching vibration for the azide group at 2110 cm^{-1}. Moreover, the chemical shift in ^1H NMR for the methylene close to the amine group match with what has been reported in the literature. Overall, our data confirm the synthesis of the amino-PEG derivatives. The diamino-PEG polymer was further reacted with FA to afford the FA-PEG-NH_2 targeting ligand (Scheme 1 and 2). Firstly, the carboxylic acid group in the FA molecule was activated by using coupling reaction in the presence of EDC and NHS. The succinimide ester derivative enhances the reactivity of the FA toward nucleophilic substitution by amines.[73] The synthesis of FA-SE was confirmed by IR and ^1H NMR. This product was dissolved in DMSO and reacted with diamino-PEG for 48 h at RT. As expected from a statistical or non-selective reaction, there is the possibility of obtaining all the possible products. To obtain the desired FA-PEG-NH_2 product, a separation procedure reported in the literature was followed.[79,80] The final mixture was transferred to a dialysis bag and the sample was dialyzed for 5 days with water. The final product was obtained by rotatory evaporation followed by lyophilization for 2 days. The characterization results by ^1H NMR and IR show that the desired compound was obtained.

3.2 Synthesis and characterization of control tetrakis(carboxy)phenyl porphyrin (C-TCPP) and redox-responsive tetrakis(carboxy)phenyl porphyrin (RR-TCPP) silane derivative

The synthesis of porphyrin-based silane derivatives has been an area of interest for more than two decades due to their wide variety of applications. Recently, tetra-substituted TCPP silsesquioxane was covalently incorporated into periodic mesoporous organosilica (PMO) thin films to study its potential uses in photocatalysis and photoelectrochemistry.[74] In another study, TCPP-PMOs were designed and displayed efficiency in catalytic hydrogen transfer reactions.[75] In this work, two novel versions of TCPP derivatives were synthesized and characterized. These molecules were employed as building blocks for the fabrication of PSilQ NPs. To synthesize the desired C-TCPP and RR-TCPP, a similar synthetic approach was followed (Schemes 3, 4 and 5). Firstly, the synthesis of TCM_4PP is realized through the reaction of benzaldehyde and pyrrole in propionic acid at 150 °C.[81] The methyl ester porphyrin then underwent hydrolysis under basic conditions in THF/EtOH to afford TCPP.[81] A distinct changed in the stretching vibration of the carbonyl from the methyl ester (1720 cm^{-1}) to the carbonyl from the carboxylic acid (1694 cm^{-1}) along with the disappearance of the methyl groups demonstrated the successful synthesis of TCPP. The next step is the conjugation of TCPP with NHS in the presence of EDC to afford the TCPP-SE molecule. The TCPP-SE derivative includes a succinimide ester which is an excellent leaving group after the nucleophilic acyl substitution with amine groups to afford the corresponding amides. This reaction was kept at 0 °C followed by warming to room temperature to avoid hydrolysis. The synthesized TCPP-SE molecule showed a distinct stretching vibration in IR corresponding to the ester and succinimide group (1736, 1770 and 1803 cm^{-1}). In addition, the appearance of the ethylene groups in ^{1}H and ^{13}C NMR provided further evidence for the successful synthesis of TCPP-SE. TCPP-SE was reacted with serine in

DMSO followed by aqueous work-up in acidic conditions to afford the amino acid form of TCPP, TCPP-Serine. The amine group of serine is a stronger nucleophile than the alcohol group, which allowed the exclusive synthesis of the amide bond, but not the ester derivative. The disappearance of the succinimide peaks from NHS and the appearance of serine's peaks in IR and NMR confirmed the synthesis of TCPP-serine. Lastly, the C-TCPP silane derivative was synthesized by reacting TCPP-Serine with TES-PI under N_2 atmosphere in anhydrous DMF for 22 h. This was followed by aqueous work-up in acidic conditions to afford C-TCPP. The solubility of C-TCPP is poor in both organic and aqueous solvents, therefore NMR was difficult to obtain. However, the IR provides some evidence for synthesis of the desired molecule. The IR shift for the carbonyl group (1706 cm^{-1}) along with the appearance of the Si-C (1233 cm^{-1}) and Si-O (1016 cm^{-1}) are an indication for a successful conversion.

The synthesis of the redox-responsive linker RR-TCPP was attempted using two different approaches as shown in Scheme 6. The first approach follows a similar protocol to the one for the synthesis of TCPP-serine. TCPP-SE was reacted with cysteine in DMSO to afford TCPP-cysteine. The premise for this first method was the previous success with the synthesis of TCPP-Serine. However, the final product was not confirmed neither by ^{1}HNMR nor MALDI. The aliphatic protons for the amino acid were not visible and the use of MALDI did not identify the cysteine derivate of TCPP (Table 1). As in the case with serine, the reaction was carried out in DMSO because this solvent easily dissolved both TCPP-SE and the amino acid; however, it was found out in the literature that cysteine can be oxidized by DMSO to form a disulfide bridge between two cysteines along with H_2O and dimethyl sulfide.[76] We hypothesize that the reaction between the

oxidized cysteine (disulfide bridged) and TCPP-SE is not successful due to steric hindrance and may also be due to intramolecular hydrogen bond between the hydrogens on the amine group and lone pairs on the sulfur atom. Therefore a second approach using TCPP-SE with pyridine disulfide cysteine hydrochloride was investigated (Scheme 6). Nevertheless, the reaction was not successful as was shown by the lack of presence of peaks for the cysteine in ^{1}HNMR. Despite different synthetic conditions used to push the reaction forward, all of them failed (Table 1). This approach was not successful presumably because the amine nucleophile from the PDSC derivative was unable to approach and react with the carbonyl from TCPP-SE due to steric hindrance.

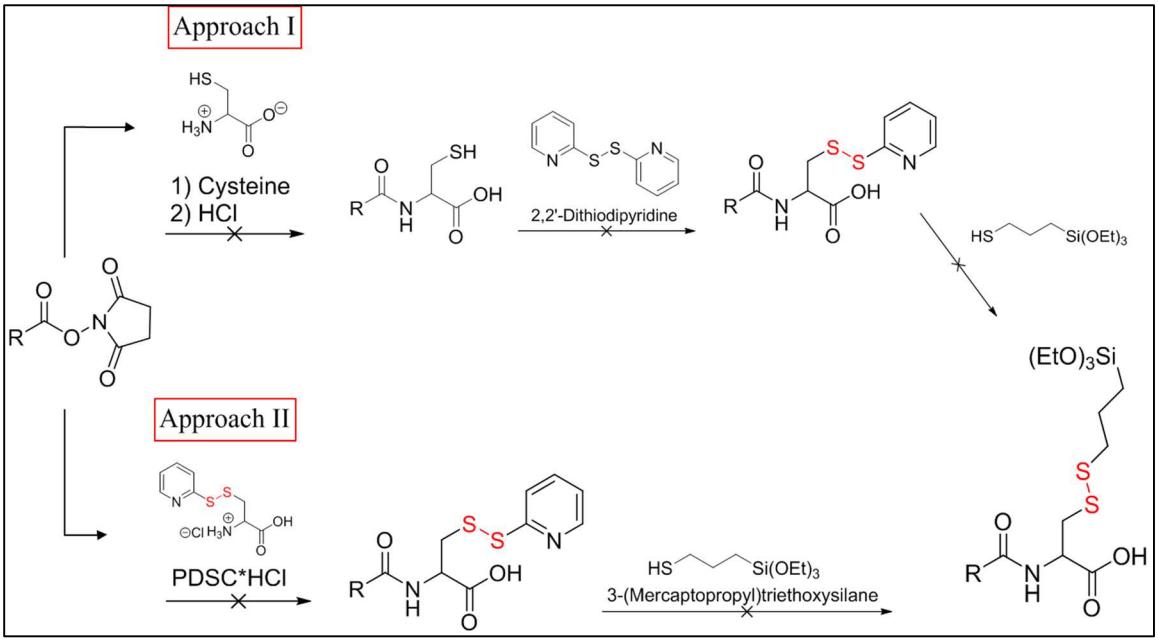

Scheme 6: Two unsuccessful synthetic approaches in pursuit of the synthesis of RR-TCPP.

Table 1: Several conditions and results using approaches I and II.

APPROACH	CONDITIONS	RESULTS
I	1) Cysteine, DIPEA, DMSO, 100 °C, 48 hrs 2) HCl	Aliphatic protons not visible in NMR Unable to visualize molecular ion with MALDI
I	1) Cysteine, DIPEA, DMSO, 120 °C, 48 hrs 2) HCl	Aliphatic protons not visible in NMR Unable to visualize molecular ion with MALDI
I	1) Cysteine, DIPEA, DMSO, 140 °C, 72 hrs 2) HCl	Aliphatic protons not visible in NMR Unable to visualize molecular ion with MALDI
II	PDSC*HCl, Et_3N, DMSO, 100 °C, 48 hrs	Aliphatic protons not visible in NMR
II	PDSC*HCl, Et_3N, DMSO, 100 °C, 72 hrs	Aliphatic protons not visible in NMR
II	PDSC*HCl, Et_3N, DMSO, 120 °C, 72 hrs	Aliphatic protons not visible in NMR
II	PDSC*HCl, Et_3N, DMSO, 120 °C, 96 hrs	Aliphatic protons not visible in NMR
II	PDSC*HCl, Et_3N, DMSO, 140 °C, 72 hrs	Aliphatic protons not visible in NMR

The successful synthesis of the redox-responsive linker was carried out following the steps depicted in Scheme 4. Firstly, TCPP-SE was reacted with PDSEA*HCl and Et_3N in DMF at 80 °C. NMR confirmed the synthesis of TCPP-PDSEA. The peaks in ^1H NMR for the succinimide group are no longer present; moreover, aromatics peaks corresponding to the pyridine group are observed. TCPP-PDSEA is further reacted through a disulfide displacement with cysteine in DMF at 60 °C. The disappearance of the peaks in ^1H NMR corresponding to pyridine and the appearance of the peaks in ^1H NMR associated to cysteine suggested the successful disulfide reaction to afford TCPP-cysteine. Lastly, TCPP-cysteine was reacted with TES-PI in anhydrous DMF under N_2 atmosphere. The final product (RR-TCPP) was worked-up in aqueous acidic conditions. The solubility of RR-TCPP is poor in both organic and aqueous solvents; therefore, this compound was not characterized by NMR and MALDI-MS. However, the IR provides

some evidence for the synthesis of the desired molecule. The IR shift for the carbonyl group (1714 cm^{-1}) along with the appearance of the Si-C (1222 cm^{-1}) and Si-O (1019 cm^{-1}) are an indication for the successful conversion.

3.3 Singlet Oxygen Generation of TCPP derivatives

In PDT, the main function of a photosensitizer is to produce $^1O_2$. To evaluate whether the successive chemical modifications of the TCPP molecule affect $^1O_2$ generation, we measured the amount of $^1O_2$ generation in TCPP (Compound 8), TCPP-Serine (Compound 10) and TCPP-EtSH (Compound 16) by using a chemical probe (Figure 11). 1,3-diphenylisobenzofuran (DPBF) was used as $^1O_2$ probe in this work. DPBF is a singlet oxygen scavenger that reacts in a diels-alder [4 + 2]-cycloaddition with the singlet oxygen generated by the excited PS. DPBF usually absorbs light at 419 nm; however, after the reaction with $^1O_2$ the resulting product does not absorb light at that wavelength. By taking advantage of this quenching assay, we can indirectly quantify the amount of $^1O_2$ generated by the TCPP derivatives. Samples of TCPP, TCPP-serine and TCPP-EtSH were prepared in DMF together with DPBF at a concentration of 2.5 μM and 5 μM, respectively. The samples were illuminated using white (400-700 nm) and red (630-700 nm) light at different intensities. The data show that the generation of $^1O_2$ by the TCPP, TCPP-serine and TCPP-EtSH after irradiation with white light does not have statistically significant differences (Figure 11a). In the case of red light, a slightly higher generation of $^1O_2$ was observed with TCPP-serine (Figure 11b). Our results showed that the production of $^1O_2$ is slightly affected by the modification of TCPP. Therefore, as long as we have the same amount of TCPP molecules in the PSilQ nanoparticles, the phototoxicity properties should be comparable.

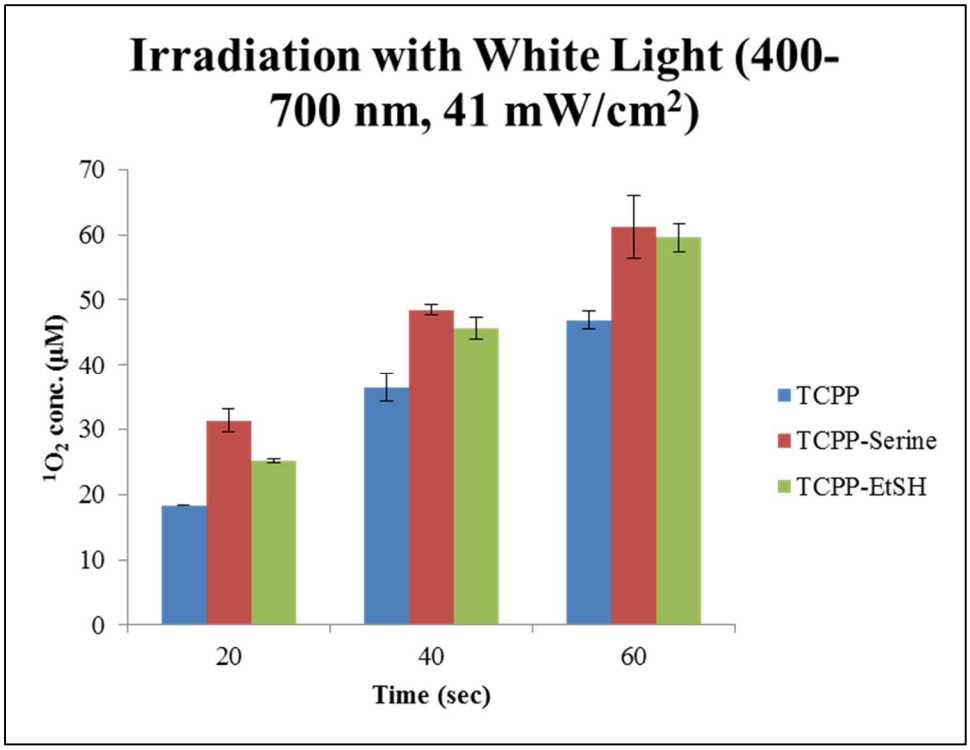

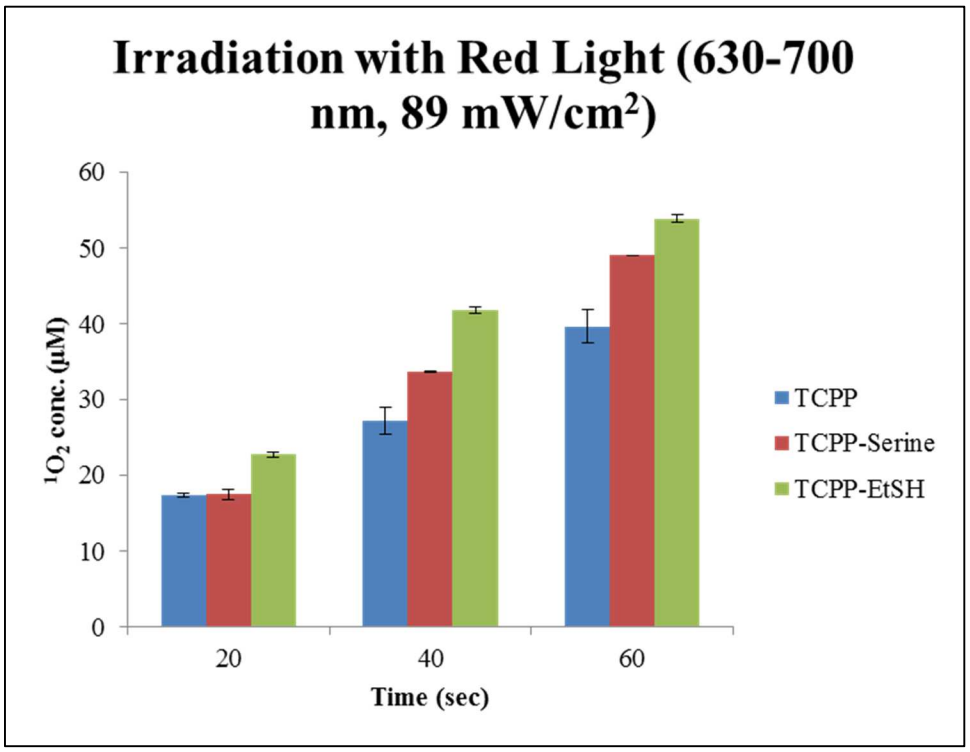

Figure 11: Singlet oxygen production using TCPP, and the two amino acid derivatives, TCPP-Serine and TCPP-Cysteine respectively.

3.4 Synthesis and characterization of TCPP-loaded multifunctional PSilQ NPs with target-specific capabilities toward cancer cells

3.4.1 PSilQ NPs; Control and Redox-responsive

The PSilQ nanoparticles in this work were synthesized by following a reverse microemulsion method composed of a quaternary system. Reverse phase microemulsions are highly tailorable systems that consist of nanometer-sized water droplets stabilized by a surfactant in a predominantly organic phase.[72] The micelles in the microemulsion essentially act as ‘‘nanoreactors’’ that assist in controlling the kinetics of particle nucleation and growth. This method allows for careful control of particle size and polydispersity. The reverse microemulsion method is superior to the Stöber method for making monodisperse silica nanoparticles smaller than 100 nm.[72] The quaternary system consists of Triton X-100, 1-hexanol, cyclohexane and C-TCPP or RR-TCPP, which are used as surfactant, co-surfactant, organic solvent and silica precursor, respectively. Firstly, the silica precursor is dissolved in water in the presence of a base (NH_4OH or NaOH) to accelerate the polymerization reaction. Previous experiences in our group with porphyrin-based silica precursors has shown the challenges to dissolve these precursors in aqueous solutions. However, in the case of C-TCPP and RR-TCPP molecules, the presence of “free” carboxylic acid groups facilitates this step because they are deprotonated under basic conditions affording carboxylates. These anionic groups increase the solubility of C-TCPP and RR-TCPP building blocks. The microemulsion reaction is carried out for 24 h at RT. After that, the PSilQ nanoparticles are obtained by centrifugation after the material has been crashed down with EtOH. The obtained red powder for C-TCPP and RR-TCPP-PSilQ NPs resemble the same color of both the C-

TCPP and RR-TCPP precursors. The structural properties of these PSilQ nanoparticles were characterized by DLS, zeta-potential, SEM and TGA. The DLS showed that the hydrodynamic diameter of C-TCPP PSilQ NPs is 1082 ± 279 and 537 ± 193 nm in EtOH and PBS, respectively. In the case of RR-TCPP PSilQ NPs, the hydrodynamic diameter is 1008 ± 296 and 685 ± 218 nm in EtOH and PBS, respectively. The colloidal stability of both C-TCPP and RR-TCPP PSilQ NPs is better in PBS than EtOH because this solution has a higher ionic strength. The presence of negative charge in the PSilQ NPs under these conditions increases the electrostatic repulsion between PSilQ NPs. It is also important to notice that the colloidal stability of this TCPP PSilQ platform has been dramatically improved in comparison with our previous PpIX PSilQ system. The zeta potential for C-TCPP and RR-TCPP PSilQ NPs in PBS was -26.1 ± 4.3 and -31.3 ± 4.0 mV, respectively. The zeta-potential measurements confirmed that the surface of the PSilQ NPs is negatively charged due to the presence of "free" carboxylates. As mentioned above, the surface charge also has a positive impact in the colloidal stability of these PSilQ particles. SEM images show that the size of C-TCPP PSilQ NPs is 40 nm in diameter (Figure 12). The amount of organic content was determined to be 20 and 35% (wt%) (Table 2) by TGA. Nevertheless; these values are way too low for what is expected for these type of materials based on the literature and our own experience. It was noticed that after running the TGA experiment, a black powder was collected, instead of the expected white powder due to the formation of SiO_2 after calcination at 800 ºC. The way that TGA determines the amount of organic content is by calculating the difference in weight after the sample has been burned out and the products of combustion (CO_2 and H_2O) left the TGA pan. In the case of C-TCPP PSilQ NPs, it appears that

instead of forming CO_2, carbon is formed. Carbon does not leave the TGA pan, which is misleading our calculations for TGA. UV-vis spectroscopy will to be used as an alternative to calculate the amount of TCPP in the nanoparticles.

3.5 Conjugation of FA-PEG and Meo-PEG to PSilQ NPs

The C-TCPP and RR-TCPP-PSilQ nanoparticles were further functionalized with MeO-PEG-NH_2 and FA-PEG-NH_2 polymers. The modification was carried out by a conjugation reaction mediated by EDC between the carboxylic acid groups in the surface of the nanoparticles and the amine groups from the PEG chains. The structural properties of the modified MeO-PEG/FA-PEG-C-TCPP and RR-TCPP PSilQ nanoparticles were characterized by DLS and zeta-potential (Table 3). The hydrodynamic diameter of MeO-PEG C-TCPP PSilQ NPs is 804 and 578 nm in EtOH and PBS, respectively. In the case of FA-PEG C-TCPP the hydrodynamic diameter is 1837 and 478 nm in EtOH and PBS, respectively. There is an increment of the hydrodynamic diameter after PEGylation because PEG polymer shields the surface charge of the nanoparticle, which reduces the electrostatic repulsion. As was expected, the surface charge of MeO-PEG and FA-PEG C-TCPP PSilQ NPs was dramatically reduced to -6.1 and 1.7, respectively.

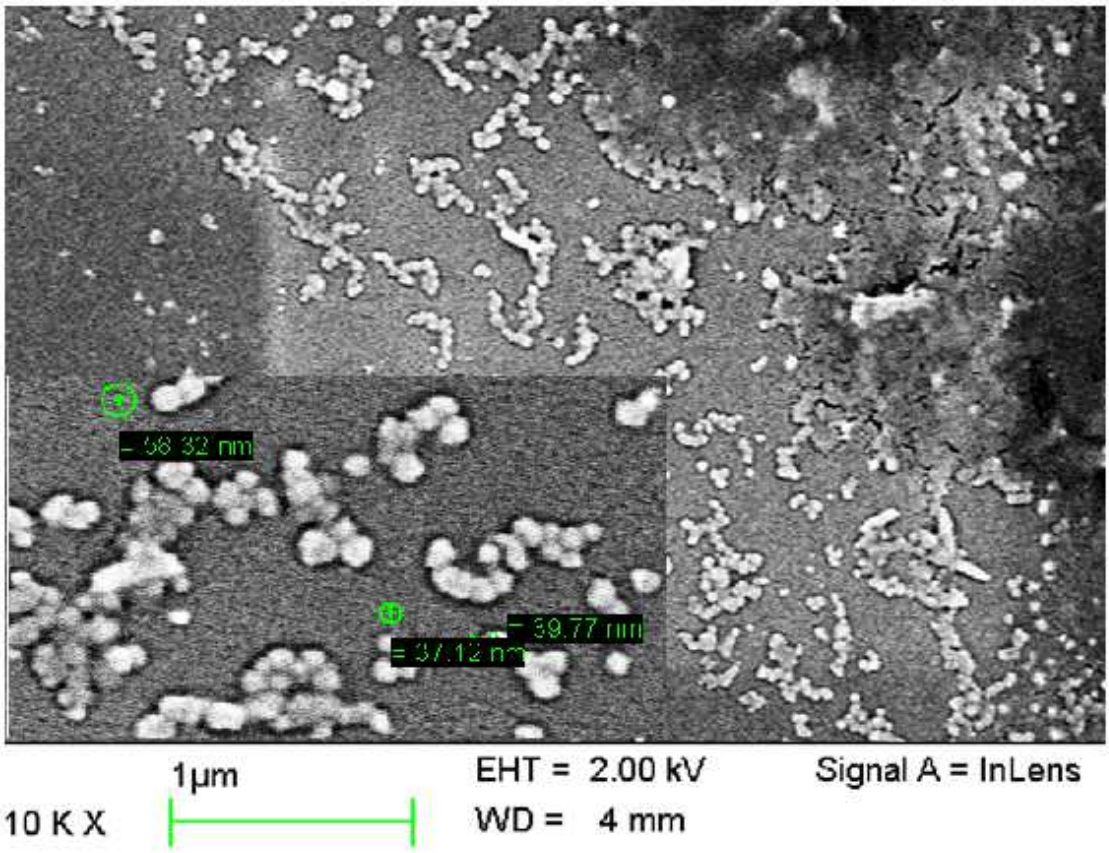

Figure 12: SEM images of C-TCPP PSilQ NPs. The inset shows a zoom-in of the NPs. The size of the NPs is ~40 nm in diameter.

Table 2: Structural properties of C-TCPP and RR-TCPP PSilQ NPs.

Sample	Hydrodynamic diameter (nm) (EtOH)	PDI	Hydrodynamic diameter (nm) (PBS)	PDI	ζ-potential (mV)	TGA (%wt)
C-TCPP PSilQ NPs	1082.6 ± 278.6	0.944	537.4 ± 192.8	0.748	-26.1 ± 4.3	19.9
RR-TCPP PSilQ NPs	1008.6 ± 296.4	0.868	684.7 ± 218.3	0.839	-31.3 ± 4.0	35.4

Table 3: Structural properties of FA-PEG and MeO-PEG C-TCPP PSilQ NPs.

Sample	Hydrodynamic diameter (nm) (EtOH)	PDI	Hydrodynamic diameter (nm) (PBS)	PDI	ζ-potential (mV)
C-TCPP MeO PEG PSilQ NPs	804.4	0.617	578.0	0.757	-6.1
C-TCPP FA PEG PSilQ NPs	1837.0	0.243	417.1	0.743	1.7

CHAPTER 4: CONCLUSIONS AND FUTURE WORK

PDT is an alternative to current treatments such as chemotherapy and radiation therapy for oncological applications. However, more efficient methods for the delivery of photosensitizers need to be developed to increase its impact in clinical settings. Degradable hybrid nanoparticles that can target cancer cells and be degraded under specific conditions are a promising approach to enhance both the loading of photosensitizers and the phototoxic effect. In this study, we have focused our efforts on developing degradable hybrid nanoparticles based on the PSilQ platform. In particular, we have used TCPP building blocks that can be degraded under reducing conditions to build PSilQ nanoparticles. This material was modified with PEG polymer that contains folic acid, a well-established targeting agent. Our approach to reach this goal was divided in three specific aims; **1)** Synthesis and characterization of FA-PEG-NH_2 and MeO-PEG-NH_2; **2)** Synthesis and characterization of the C-TCPP and RR-TCPP silane derivatives; and **3)** Synthesis and characterization of target-specific TCPP-loaded PSilQ NPs.

The synthesis of FA-PEG-NH_2 and MeO-PEG-NH_2 was carried out following protocols already reported in the literature.[77-80] PEG and MeO-PEG materials were converted to their corresponding amine derivatives by introducing azido moieties followed by a mild reduction using the Staudinger conditions. To afford FA-PEG-NH_2, the diamino-PEG chain was reacted with the activated FA-SE. The crude mixture of FA-PEG-NH_2 was purified to obtain the mono-substituted product by using a dialysis bag in water as was previously reported. The products obtained in the different steps of the synthesis were characterized by FTIR and ^{1}H NMR. The data obtained was consistent with the

characterization results previously reported in the literature. This confirmed the successful synthesis of FA-PEG-NH_2 and MeO-PEG-NH_2. These PEG-polymer chains were used to modify the surface properties of the PSilQ nanoparticles.

The novel C-TCPP and RR-TCPP silane derivatives were synthesized via multi-step synthetic pathway. For the first part of the synthesis, up to TCPP-SE, we followed procedures already reported in the literature with some modifications.[81] TCPP-SE was reacted with serine to afford TCPP-serine. TCPP-serine was further reacted with the silane precursor, TES-PI to obtain the desired C-TCPP. The different steps for the synthesis of C-TCPP were characterized by IR, NMR and MALDI-MS when the solubility of the compounds allowed it. To obtain TCPP-cysteine, the same approach as the one for serine was followed; however, this synthetic strategy did not work in the case of cysteine. Presumably, due to the formation of cysteine dimers after oxidation in DMSO, which inhibits by steric effects the nucleophilic attach of the amine group. An alternative approach was designed where TCPP-SE was reacted with pyridine-disulfide cisteamine to afford TCPP-PDSEA. This compound was further reacted with cysteine by a disulfide exchange followed by the reaction with TES-PI to afford the desired RR-TCPP molecule. The products in each step of the reaction were characterized by FTIR, ^{1}H NMR, ^{13}C NMR, UV-vis spectroscopy and MALDI-TOF when the solubility of the TCPP molecules allowed it. As far as we know, both C-TCPP and RR-TCPP are novel pophyrin-based silane derivatives that has not been reported in the literature. It is important to point out that it was found that the synthesis of these TCPP-derivatives resulted in a mixture of mono, di, tri and tetra-substituted products. The purification of these mixtures was not further pursued in this work. We hypothesized that for the

synthesis of TCPP-PSilQ nanoparticles the presence of TCPP building blocks with different degree of substitution will not dramatically affect the final structural and photophysical properties of the desired materials. Moreover, it was observed that the $^1O_2$ production of TCPP versus some of the modified TCPP derivatives (TCPP-serine and TCPP-EtSH) was comparable. Therefore, it was concluded that a mixture of TCPP building blocks with different degrees of substitution does not have any major effect on the phototoxic capabilities of the PSilQ nanoparticles fabricated in this work.

The PSilQ NPs were synthesized using a reverse-microemulsion method already reported in the literature. The process involves an organic phase comprised of a surfactant/co-surfactant, and an aqueous phase with the dissolved PS silica precursor. The structural properties were determined using DLS, ζ-potential and SEM. Both C-TCPP and RR-TCPP PSilQ particles showed similar colloidal stability under physiological conditions. Moreover, as expected, the surface charge is highly negative due to the presence of "free" carboxylates in the surface of the nanoparticles. SEM images confirmed the successful synthesis of spherical nanoparticles with a diameter of 40 nm. Finally, C-TCPP PSilQ NPs were functionalized with MeO-PEG-NH_2 and a mixture of FA-PEG-NH_2/MeO-PEG-NH_2 polymers. The structural properties of the PEGylated PSilQ materials were determined by using DLS and ζ-potential. As anticipated, an increase in the hydrodynamic diameter for the PEGylated materials was observed due to the shielding of the negative charge in the presence of PEG chains. This effect was confirmed by the shift in the zeta-potential toward neutral values for all the PEGylated materials.

Future work

The issues with the quantification of TCPP loading in the PSilQ particles by TGA need to be addressed. Some alternatives for the quantification of TCPP or silane molecules are UV-vis spectroscopy or OES-MS, respectively. The photophysical properties of the PSilQ NPs such as UV-vis, fluorescence and $^1O_2$ generation have to be determined. Moreover, the stimuli-responsive properties of the RR-TCPP-PSilQ nanoparticles need to be further characterized in solution in the presence of a reducing agent and compared with the control sample. Previous reports from our group have shown that similar PSilQ nanoparticles containing redox-responsive protophorpyrin-IX derivatives as PS agent are degraded under high reducing environment. We envision that a similar performance will be obtained for the PSilQ platform developed in this project. Finally, the *in vitro* properties of these nanoparticles need to be tested with different cancer cell lines. The cytotoxicity in the absence and presence of light will be tested by the MTS assay. The target-specificity of the FA-PEG PSilQ NPs will be evaluated by flow cytometry using cancer cells that overexpress folate receptors such as HeLa or colon cancer cell lines. The internalization and final fate of the nanoparticles will be determined by confocal microscopy. Hela cell lines, breast and colon cancer cell lines are some alternatives to be used for characterizing the *in vitro* performance of the TCPP PSilQ platform.

REFERENCES

1. Cancer Facts and Figures 2015, *American Cancer Society*, **2015**, 1-54.

2. Choi, K.; Liu, G.; Lee, S.; Chen., Theranostic nanoplatforms for simultaneous cancer imaging and therapy: current approaches and future perspectives. *Nanoscale*, **2012**, *4*, 330-342.

3. Triesscheijn, M.; Baas, P.; Schellens, J.; Stewart, F., Photodynamic Therapy in Oncology. *The Oncologist*, **2006**, *11*, 1034-1044.

4. Allision. R.; Moghissi, K., Photodynamic Therapy (PDT): PDT Mechansim. *Clinical Endoscopy*, **2013**, *46*, 24-29.

5. Hopper, C., Photodynamic therapy: a clinical reality in the treatment of cancer. *THE LANCET Oncology*, **2000**, *1(4)*, 212-219.

6. Ethirajan, M.; Chen, Y.; Joshi, P.; Pandey, R., The role of porphyrin chemistry in tumor imaging and photodynamic therapy. *Chemical Society Reviews*, **2011**, *40*, 340-362.

7. Ackroyd, R.; Kelly, C.; Brown, N.; Reed, M., The history of photodynamic therapy and photodetection. *Photochemistry and Photobiology*, **2001**, *74(5)*, 656-669.

8. Ackroyd, M., A brief overview of photodynamic therapy in Europe. *Photodiagnosis and photodynamic therapy*, **2008**, *5(2)*, 103-111.

9. Dennis, E.; Dolmans, G.; Fukumura, D.; Jain, R., Photodynamic therapy for cancer. *Nature Reviews Cancer*, **2003**, *3*, 380-387.

10. Pinton, P.; Szeimies, B.; Ortel, B., Photodynamic Therapy and Fluorescence Diagnosis in Dermatology. **2001**.

11. Kelly, J.; Snell, M.; Berenbaum, M., Photodynamic destruction of human bladder carcinoma. *British Journal of* Cancer, 1975, *31(2)*, 237-244.

12. Brown, S., Photodynamic therapy for photochemists. *Philosophical Transactions Of The Royal Society A*, **2013,** *371*, 1-16.

13. Ethirajan, M.; Chen, Y.; Joshi, P.; Pandey, R., The role of porphyrin in tumor imaging and photodynamic therapy. *Chemical Society Reviews*, **2011,** *40*, 340-362.

14. Juarranz, A.; Jaen, P.; Rodriguez-Sanz, F.; Cuevas, J.; Gonzalez, S., Photodynamic therapy of cancer. Basic principles and applications. *Clinical Translational Oncology*, **2008**, *10*, 148-154.

15. Brown, S.; Brown, E.; Walker, I., The present and future role of photodynamic therapy in cancer treatment. *Lancet Oncology*, **2004**, *5(8)*, 497-508.

16. Dougherty, T.; Gomer, C.; Henderson, B.; Jori, G.; Kessel, D.; Korbelik, M.; Moan, J.; Peng, Q., Photodynamic Therapy. *Journal of the National Cancer Institute*, **1998**, *90(12)*, 889-905

17. Ormond, A.; Freeman, H., Dye Sensitizers for Photodynamic Therapy. *Materials* **2013**, *6(3),* 817-840.

18. Paszko, E., Ehrhardt, C., Senge, M., Kelleher, D., Reynolds, J., Nanodrug applicaions in photodynamic Therapy. *Photodiagnosis and Photodynamic Therapy*, **2011,** *8*, 14-29.

19. Bechet, D.; Couleaud, P.; Frochot, C.; Viriot, M.; Guillemin, F.; Barberi-Heyob, M., Nanoparticles as vehicles for delivery of photodynamic therapy agents. *Trends in Biotechnology*, **2008,** *26(11)*, 612-621.

20. Josefsen, L.; Boyle, R., Unique Diagnostic and Therapeutic Roles of Porphyrins and Phthalocyanines in Photodynamic Therapy, Imaging and Theranostics. *Theranostics*, **2012,** *2(9)*, 916-966.

21. Nayak, C., Photodynamic therapy in dermatology. *Indian Journal of Dermatology Venereology Leprology*, **2005**, *71(3)*, 145-220.

22. Mang, T., Lasers and light sources for PDT: past, present and future. *Photodiagnosis and Photodynamic Therapy*, **2004**, *1(1)*, 43-48.

23. Mayeda, E.; Bard, A., Production of singlet oxygen in electrogenerated radical ion electron transfer reactions. *Journal American Chemical Society*, **1973**, *95 (19)*, 6223-6226.

24. DeRosa, M.; Crutchley, R., Photosensitized singlet oxygen and its applications. *Coordination Chemistry Reviews*, **2002**, *233-234*, 351-371.

25. Niedre, M.; Patterson, M.; Wilson, B., Direct Near-infrared Luminescence Detection of Singlet Oxygen Generated by Photodynamic Therapy in Cells *In*

Vitro and Tissues *In Vivo*. Photochemistry *and Photobiology*, **2002**, *75(4)*, 382–391.

26. Oleinick, N.; Morris, R.; Belichenko, I., The role of apoptosis in response to photodynamic therapy: what, where, why, and how. *Photochemistry Photobiology Science*, **2002**, 1, 1–21.

27. Apel, K.; Hirt, H., REACTIVE OXYGEN SPECIES: Metabolism, Oxidative Stress, and Signal Transduction. *Annual Review of Plant Biology*, **2004**, *55*, 373-399.

28. Castrano, A.; Demidova, T.; Hamblin, M., Mechanisms in photodynamic therapy: part one-photosensitizers, photochemistry and cellular localization. *Photodiagnosis and Photodynamic Therapy*, **2004**, *1(4)*, 279-293.

29. Dolphin, D., The porphyrins. **1978-1979**, *1*.

30. Sternberg E.; Dolphin, D., Pyrrolic Photosensitizers. *Current Medicinal Chemsitry*, **1996**, *3*, 239-272.

31. Ali, H.; van Lier, J., Metal Complexes as Photo-and Radiosensitizers. *Chemical Reviews*, **1999**, *99(9)*, 2379-2450.

32. Comuzzi, C.; Cogoi, S.; Overhand, M; Van der Marel, G.; Overkleeft, H.; Xodo, L., Synthesis and Biological Evaluation of New Pentaphyrin Macrocycles for Photodynamic Therapy. *Journal of Medicinal Chemistry*, **2006**, *49(1)*, 196-204.

33. The oxford english dictionary, **2015**.

34. O'Connor, A.; Gallagher, W.; Byrne, A., Porphyrin and Nonporphyrin Photosensitizers in Oncology: Preclinical and Clinical Advances in Photodynamic Therapy. *Photochemistry and Photobiology*, **2009**, *85* (5), 1053-1074.

35. Allison, R.; Moghissi, K., Photodynamic Therapy (PDT): PDT Mechanisms. *Clinical Endoscopy*, **2013**, *46(1)*, 24-29.

36. Nyman, E.; Hynninen, P., Research advances in the use of tetrapyrrolic photosensitizers for photodynamic therapy. *Journal of Photochemistry and Photobiology B: Biology*, **2004**, *73(1)*, 1-28.

37. Yano, S.; Hirohara, S.; Obata, M.; Hagiya, Y.; Ogura, S.; Ikeda, A.; Kataoka, H.; Tanaka, M.; Joh, T., Current states and future views in photodynamic therapy. *Journal of Photochemistry and Photobiology C: Photochemistry Reviews*, **2011**, *12(1)*, 46-67.

38. Zhang, Y.; Lovell, J., Porphyrins as Theranostic Agents from Prehistoric to Modern Times. *Theranostics*, **2012**, *2(9)*, 905-915.

39. Berlanda, J.; Kiesslich, T.; Engelhardt, V.; krammer, B.; Plaetzer, K., Comparative *in vitro* study on the characterisitcs of different photosensitizers employed in PDT. *Journal of Photochemistry and Photobiology B: Biology*, **2010**, *100(3)*, 173-180.

40. Josefsen, L.; Boyle, R., Unique Diagnostic and Therapeutic Roles of Porphyrins and Phthalocyanines in Photodynamic Therapy, Imaging and Theranostics. *Theranostics*, **2012**, *2(9)*, 916-966.

41. Triesscheijn, M.; Baas, P.; Schellens, J.; Stewart, F., Photodynamic Therapy in Oncology. *The Oncologist*, **2006**, *11*, 1034-1044.

42. Mitra, S.; Foster, T., Photophyscial Parameters, Photosensitizer Retention and Tissue Optical Properties Completely Account for the Higher Photodynamic Efficacy of meso-Tetra-Hydroxyphenyl-Chlorin vs Photofrin. *Photochemistry and Photobiology*, **2005**, *81(4)*, 849-859.

43. Allison, R.; Sibata, C., Oncologic photodynamic therapy photosensitizers: A clinical review. *Photodiagnosis and Photodynamic Therapy*, **2010**, *7(2)*, 61-75.

44. Vivero-Escoto, J.; Vega, D., Stimuli-responsive protoporphyrin IX silica-based nanoparticles for photodynamic therapy *in vitro*. *Royal Society of Chemistry Advances*, **2014,** *4*, 14400-14407.

45. Berg, K., Selbo, P., Weyergang, A., Dietze, A., Prasmickaite, L., Bonsted, A., Engesaeter, B., Angell-Petersen, E., Warloe, T., Frandsen, N., Hogset, A., Porphyrin-related photosensitizers for cancer imaging and therapeutic applications. *Journal of Microscopy*, **2005,** *218(2)*, 133-147.

46. Kormelli, T.; Yamauchi, P.; Lowe, N., Topical photodynamic therapy in clinical dermatology. *British Journal of Dermatology*, **2004**, *150(6)*, 1061-1069.

47. Wachowska, M.; Muchowicz, A.; Firczuk, M.; Gabrysiak, M.; Winiarska, M.; Wanczyk, M.; Bojarczuk, K.; Golab, J., Aminolevulinic Acid (ALA) as a Prodrug in Photodynamic Therapy of Cancer. *Molecules*, **2011**, *16*, 4140-4164.

48. Ishizuka, M.; Abe, F.; Sano, Y.; Takahashi, K.; Inoue, K.; Nakajima, M.; Kohda, T.; Komatsu, N.; Ogura, S., Novel development of 5-aminolevulinic acid (ALA) in cancer diagnoses and therapy. *International Immunopharmacology*, **2011**, *11(3)*, 358–365.

49. Hudson, R.; Carcenac, M.; Smith, K.; Madden, L.; Clarke, O.; Pelegrin, A.; Boyle, R., The development and characterization of porphyrin isothiocyanate-

monoclonal antibody conjugates for photoimmunotherapy. *British Journal of Cancer*, **2005**, *92*, 1442 – 1449.

50. Taquet, J.; Frochot, C.; Manneville, V.; Barberi-Heyob, M., Phthalocyanines Covalently Bound to Biomolecules for a targeted Photodynamic Therapy. *Current Medicinal Chemistry*, **2007**, *14(15)*, 1673-1687.

51. Olivo, M.; Bhuvaneswari, R.; Lucky, S.; Dendukuri, N.; Thong, P., Targeted Therapy of Cancer Using Photdynamic Therapy in Combination with Mutli-faceted Anti-Tumor Modalities. *Pharmaceuticals*, **2010**, *3(5)*, 1507-1529.

52. Polo, L.; Valduga, G.; Jori, G.; Reddi, E., Low-density lipoprotein receptors in the uptake of tumour photosensitizers by human and rat transformed fibroblasts. *International Journal of Biochemistry and Cell Biology*, **2002**, *34(1)*, 10-23.

53. Sehgal, I.; Sibrian-Vazquez, M.; Vicente, M., Photoinduced Cytotoxicity and Biodistribution of Prostate Cancer Cell-Targeted Porphyrins. *Journal of Medicinal Chemistry*, **2008**, *51(19)*, 6014-6020.

54. Bullous, A.; Alonso, C.; Boyle, R., Photosensitizer-anitbody conjugates for photodynamic therapy. *Photochemical and Photobiological Sciences*, **2011**, *10*, 721-750.

55. Master, A.; Livingston, M.; Gupta, A., Photodynamic nanomedicine in the treatment of solid tumors. *Journal of Controlled Release*, **2013**, *168(1)*, 88-102.

56. Agostinis, P.; Berg, K.; Cengel, K.; Foster, T.; Girotti, A.; Gollnick, S.; Hahn, S.; Hamblin, M.; Juzeniene, A.; Kessel, D.; Korbelik, M.; Moan, J.; mroz, P.; Nowis, D.; Piette, J.; Wilson, B.; Golab, J., Photodynamic therapy of cancer: An update. *CA: A Cancer Journal for Clinicians*, **2011**, *61(4)*, 250–281.

57. Danhier, F.; Feron, O.; Preat, V., To exploit the tumor microenvironment: Passive and active tumor targeting of nanocarriers for anti-cancer drug delivery. *Journal of Controlled Release*, **2010**, *148(2)*, 135–146.

58. Bertrand, N.; Wu, J.; Xu, X.; Kamaly, N.; Farokhzad, O., Cancer nanotechnology: The impact of passive and active targeting in the era of modern cancer biology. *Advanced Drug Delivery Reviews*, **2014**, *66*, 2–25.

59. Taurin, S.; Nehoff, H.; Greish, K., Anticancer nanomedicine and tumor vascular permeability; Where is the missing link? *Journal of Controlled Release*, **2012**, *164(3)*, 265–275.

60. Cheng, Z.; Zaki, A.; Hui, J.; Muzykantov, V.; Tsourkas, A., Multifunctional Nanoparticles: Cost Versus Benefit of Adding Targeting and Imaging Capabilities. *Science*, **2012**, *338*, 903-910.

61. Chouikrat, R.; Seve, A.; Vanderesse, R.; Benachour, H.; Barberi-Heyob, M.; Richeter, S.; Raehm, J.; Verelst, M.; Frochot, C., Non Polymeric Nanoparticles for Photodynamic Therapy Applications: Recent Developments. *Current Medicinal Chemistry*, **2012,** *19*, 781-792.

62. Lim, C.; Heo, J.; Shin, S.; Jeong, K.; Seo, Y.; Jang, W.; Park, S.; Kim, S.; Kwon, I., Nanophotosensitizers toward advanced photodynamic therapy of Cancer. *Cancer Letters*, **2013,** *2*, 176-187.

63. Ding, H.; Sumer, B.; Kessinger, C.; Dong, Y.; Huang, G.; Boothman, D.; Gao, J., Nanoscopic micelle delivery improves the photophysical properties and efficacy of photodynamic therapy of protoporhyrin IX. *Journal of Controlled Release*, **2011**, *151(3)*, 271–277.

64. Tu, J.; Wang, T.; Shi, W.; Wu, G.; Tian, X.; Wang, Y.; Ge, D.; Ren, L., Multifunctional ZnPc-loaded mesoporous silica nanoparticles for enhancement of photodynamic therapy efficacy. *Biomaterials*, **2012**, *33(31)*, 7903-7914.

65. Ambrogio, M.; Thomas, C.; Zhao,Y.; Zink, J.; Stoddart, J., Mechanized Silica nanoparticles: A New Frontier in Theranostic Nanomedicine. *Accounts of Chemical Research*, **2011**, *44(10)*, 903–913.

66. Oh, I.; Min, H.; Li, L.; Tran, T.; Lee, Y.; Kwon, I.; Choi, K.; Kim, K.; Huh, K., Cancer cell-specific photoactvity of pheophorbide a-glycol chitosan nanoparticles for photodynamic therapy in tumor-bearing mice. *Biomaterials*, **2013**, *34(27)*, 6454-6463.

67. Preuss, A.; Chen, K.; Hackbarth, S.; Wacker, M.; Langer, K.; Roeder, B.: Photosensitizer loaded HSA nanoparticles II: In vitro investigations. *International Journal of Pharmaceutics*, **2011**, *404*, 308-316.

68. Vivero-Escoto, J., DeCillis, D., Fritts, L., Vega, D., Porphyrin-based polysilsesquioxane nanoparticles to improve photodynamic therapy for cancer treatment. *Proc. SPIE, Optical Methods for Tumor Treatment and Detection: Mechanisms and Techniques in Photodynamic Therapy XXIII*, **2014,** *8931*, 89310Z-1-10.

69. Chan, R.; Marcal, H.; Russell, R.; Holden, P.; Foster, L., Application of Polyethylene Glycol to Promote Cellular Biocompatibility of Polyhydroxybutyrate Films. *International Journal of Polymer Science*, **2011,** *2011*, 1-9.

70. Jokerst, J.; Lobovkina, T.; Zare, R.; Gambhir, S., Nanoparticle PEGylation for imaging and therapy. *Nanomedicne (London)*, **2011,** *6(4)*, 715-728.

71. Cal, P.; Frade, R.; Chudasama, V.; Cordeiro, C.; Caddick, S.; Gois, P., Targeting cancer cells with folic acid-iminoboronate fluorescent conjugates. *Royal Society of Chemistry Chemistry Communications*, **2014,** *50*, 5261-5263.

72. Taylor-Pashow, K.; Rocca, J.; Huxford, R.; Lin, W., Hybrid nanomaterials for biomedical applications. *Royal Society of Chemistry Chemistry Communications*, **2010,** *46*, 5832-5849.

73. Atkinson, S.; Bettinger, T.; Seymour, L.; Behr, J.; ward, C., Conjugation of Folate via Gelonin Carbohydrate Residues Retains Ribosoaml-inactivating Properties of the Toxin and Permits Targeting to Folate receptor Positive Cells. *The Journal of Biological Chemistry*, **2001**, *276*, 27930-27935.

74. Li, Y.; Auras, F.; Lobermann, F.; Doblinger, M.; Schuster, J.; Peter, L.; Trauner, D.; Bein, T., A Photoactive Porphyrin-Based Periodic Mesoporous Organosilica Thin Film. *Journal American Chemistry Society*, **2013**, *135(49)*, 18513-18519.

75. Jeong, E.; Burri, A.; Lee, S.; Park, S., Synthesis and catalytic behavior of tetrakis(4-carboxyphenyl) porphyrin-periodic mesoporous organosilica. *Journal Material Chemistry*, **2010**, *20*, 10869-10875.

76. Papanyan, Z.; Markarian, S., Detection of Oxidation of L-cysteine by Dimethyl Sulfoxide in Aqueous Solutions by IR Spectroscopy. *Journal Applied Spectroscopy*, **2013**, *80(5)*, 775-778.

77. Kikkeri, R.; Lepenies, B.; Adibekian, A.; Laurino, P.; Seeberger, P., *In Vitro* Imaging and *In Vivo* Liver Targeting with Carbohydrate Capped Quantum Dots. *Journal American Chemical. Society,* **2009**, *131(6),* 2110-2112.

78. Rocca, J.; Huxford, R.; Comstock-Duggan, E.; Lin, W., Polysilsesquioxane Nanoparticles for Targeted Platin-Based Cancer Chemotherapy by Triggered Release. *Angewandte Chemie International Edition,* **2011**, *50(44),* 10330-10334.

79. Patil, Y.; Toti, U.; Khdair, A.; Ma, L.; Panyam, J., Single-step surface functionalization of polymeric nanoparticles for targeted drug delivery. *Biomaterials,* **2009**, *30(5),* 859-866.

80. Mahalwar, A.; Sharma, A.; Sahu, R.; Rathore, D., Evaluation of Receptor Mediated Endocytosis on Cellular Internalization: A comparative Study of PEGylated Nanoparticles and Folate Anchored PEGylated Nanoparticles on MDA-MB-231 Cells. *International Journal of Biological and Pharmaceutical Research,* **2012**, *3(3),* 431-443.

81. Walter, M.; Wamser, C.; Ruwitch, J.; Zhao, Y.; Braden, D.; Stevens, M.; Denman, A.; Pi, R.; Rudine, A.; Pessiki, P., Synthesis and optoelectronic properties of amino/carboxyphenylporphyrin for potential use in dye-sensitized TiO_2 solar cells. *Journal of Porphyrins and Phthalocyanines*, **2007**, *11(8)*, 601-612.

APPENDIX:FIGURES

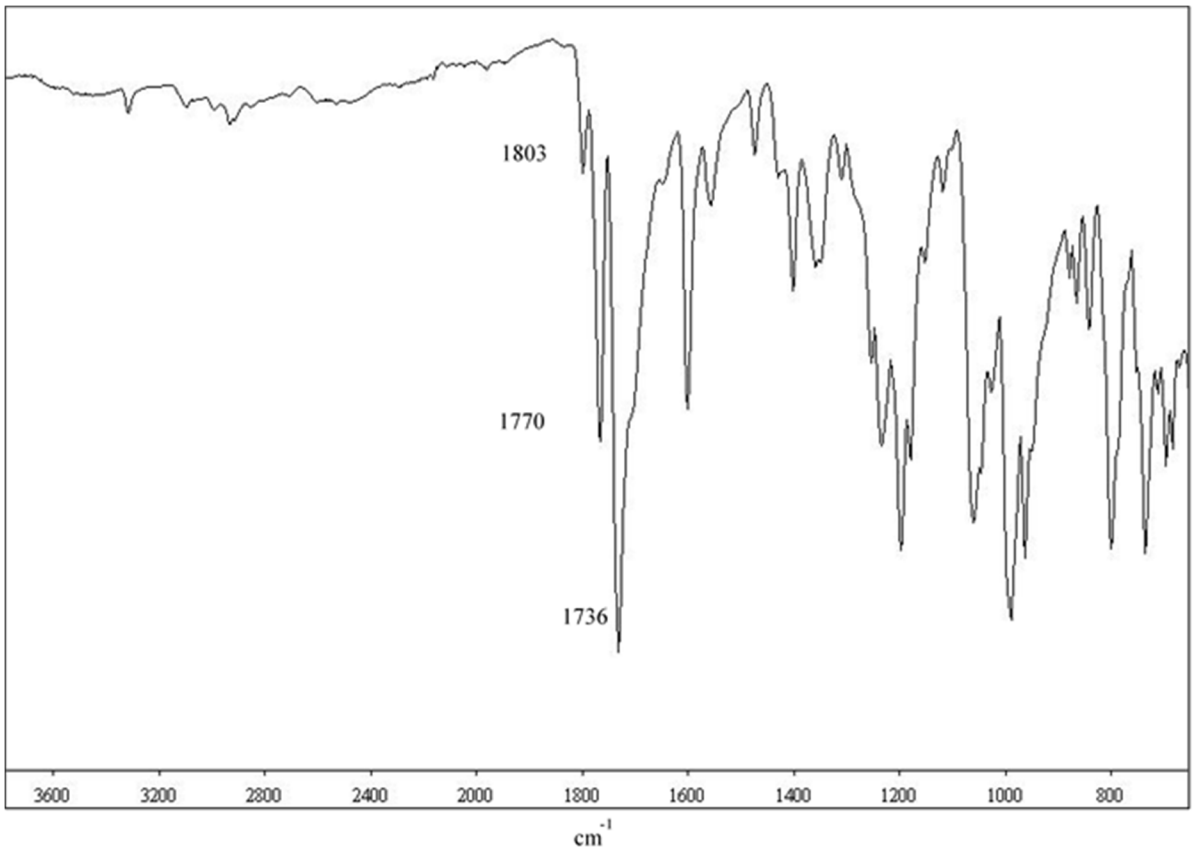

Figure A1.1: FT-IR spectra of succinimide ester of TCPP (9). IR: 1736 cm^{-1} (ester), 1770 cm^{-1} (NHS) and 1803 cm^{-1} (NHS).

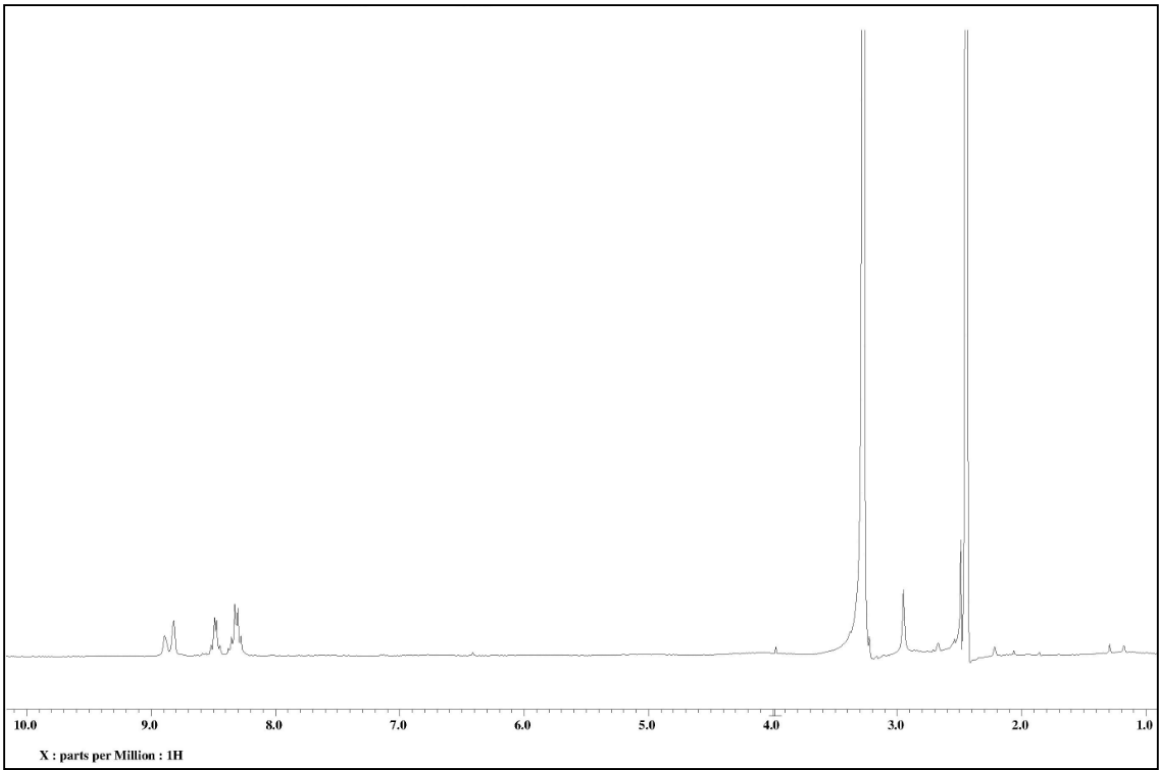

Figure A1.2: [1]HNMR spectra for succinimide ester of TCPP (9).

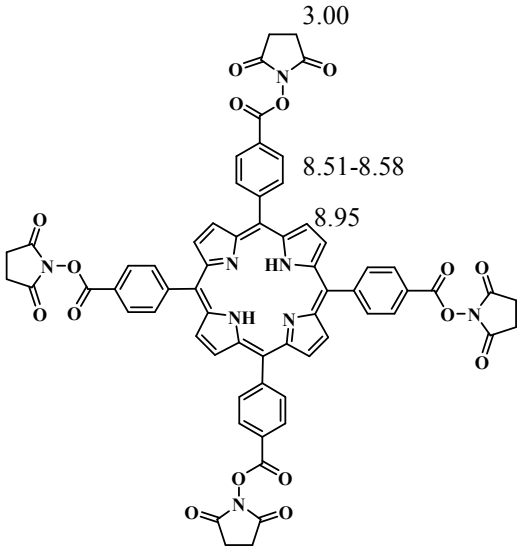

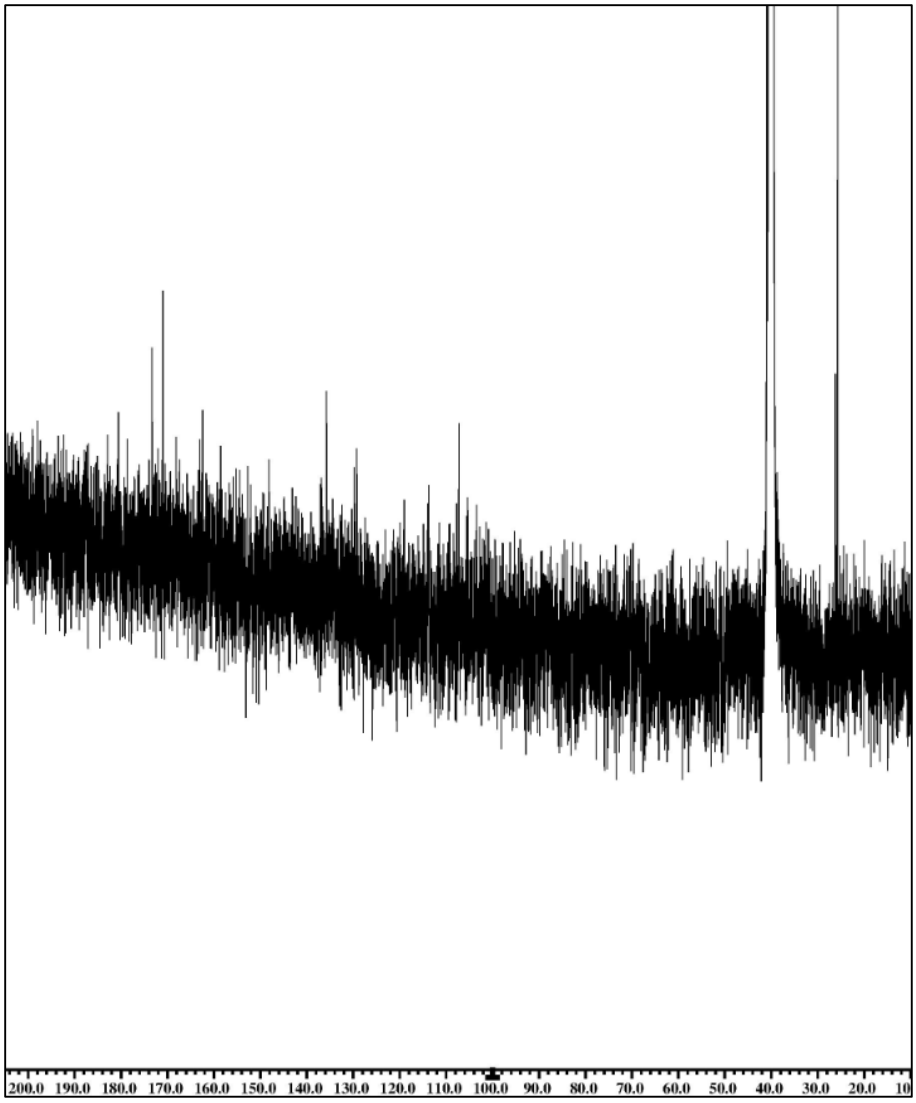

Figure A1.3: ^{13}CNMR spectra for succinimide ester of TCPP (9).

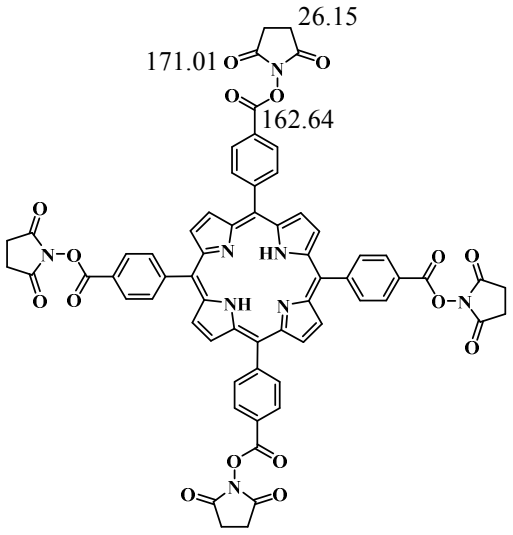

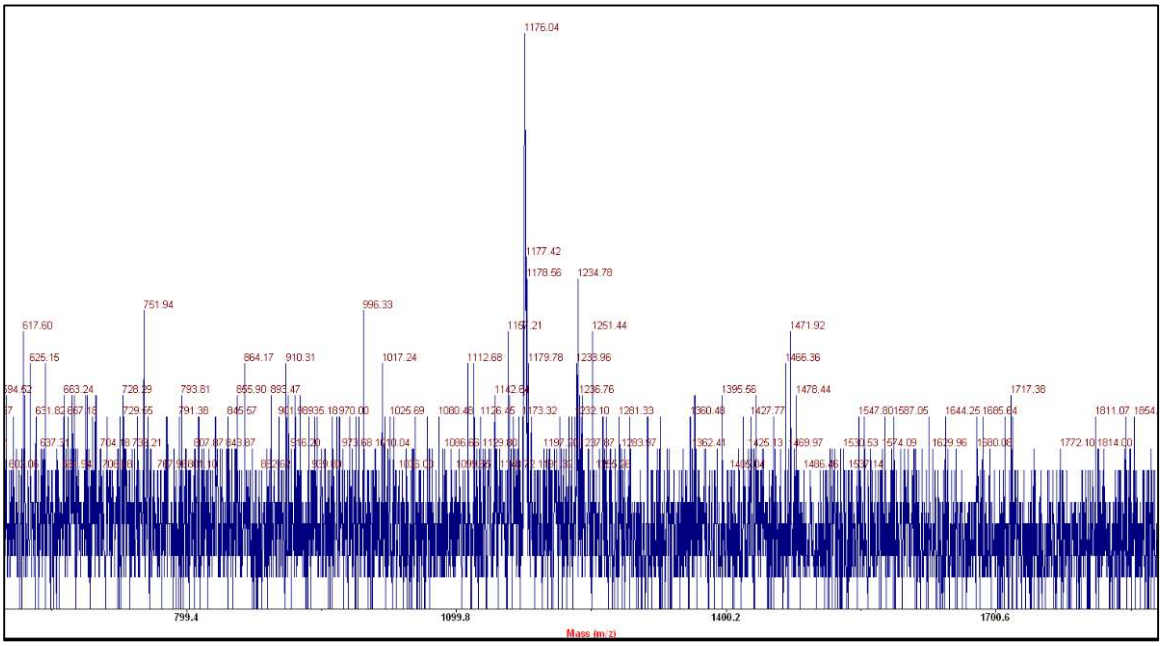

Figure A1.4: MALDI-TOF for succinimide ester of TCPP (9). M/Z, 1176.04 $[M + 1]^+$, 1177.42 $[M + 2]^+$ and 1178.56 $[M + 3]^+$.

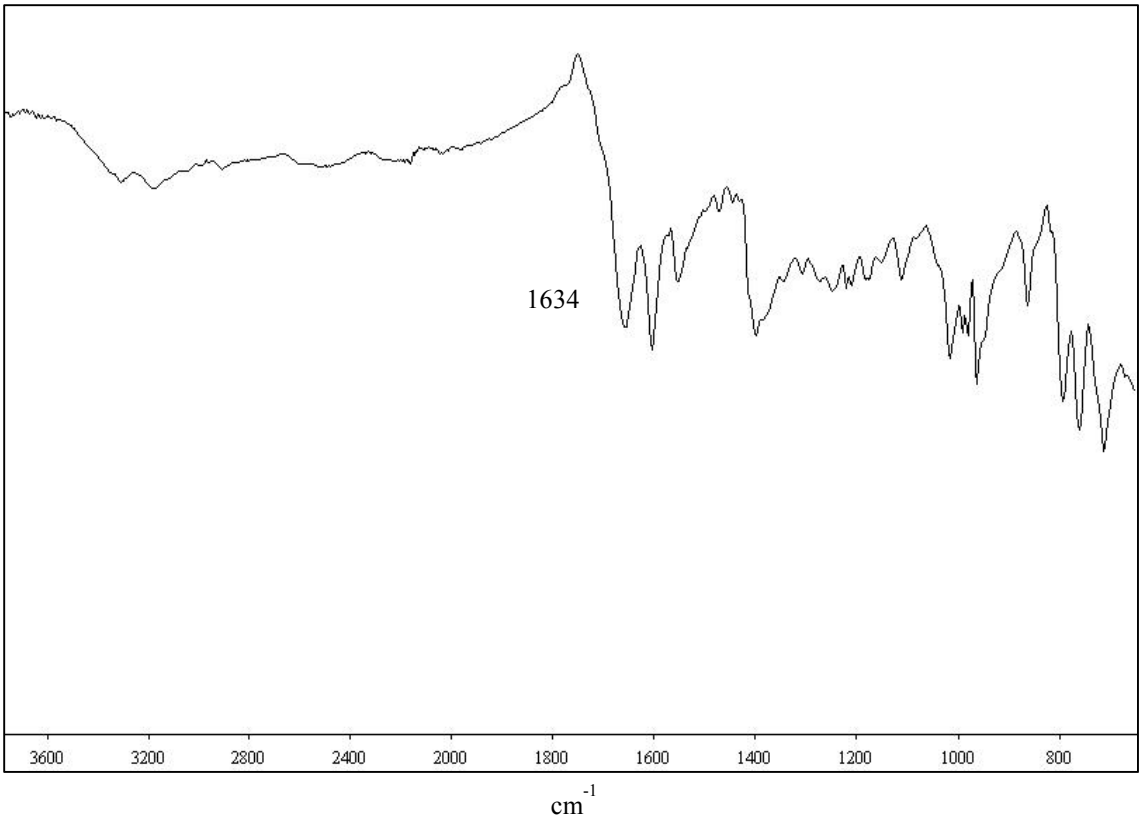

Figure A1.5: FT-IR spectra for TCPP serine derivative (10). IR: 1634 cm^{-1} (amide).

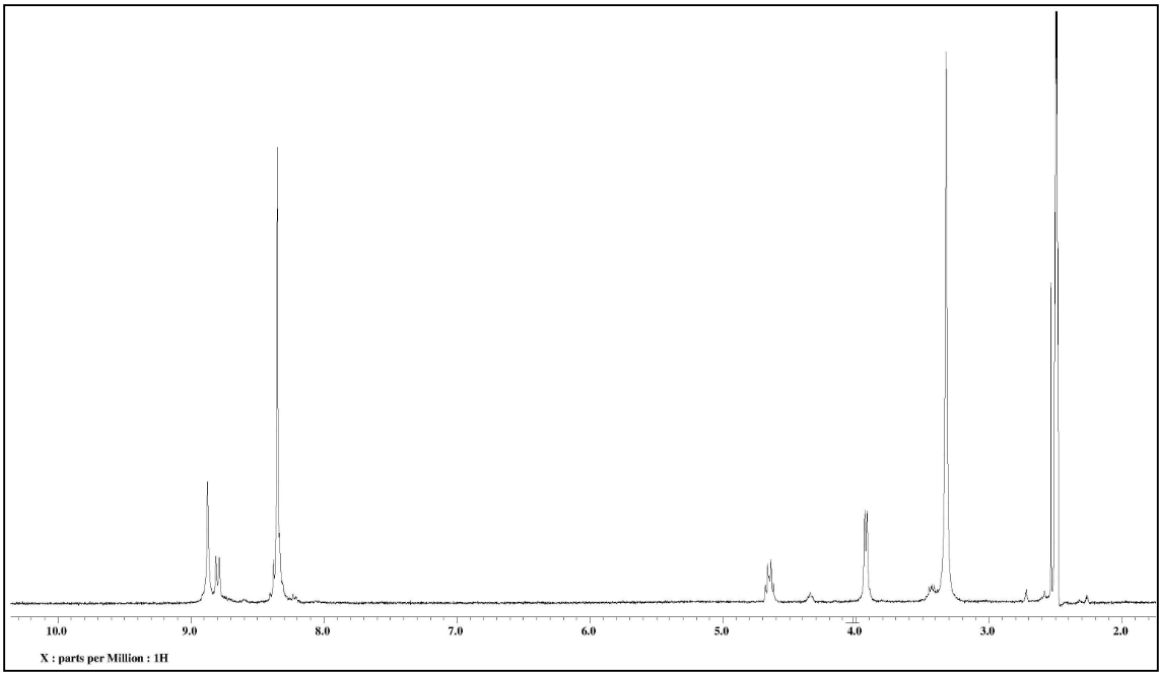

Figure A1.6: [1]HNMR spectra for TCPP serine derivative (10).

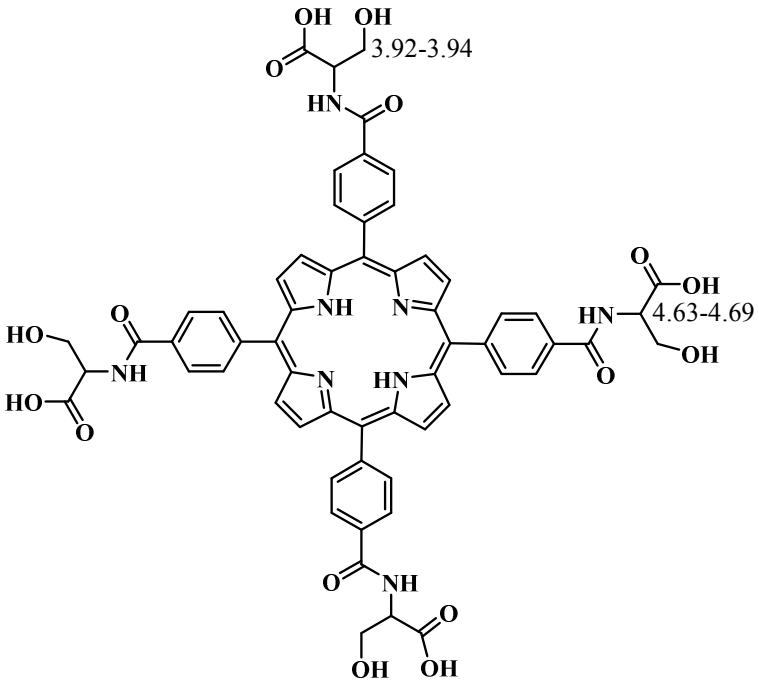

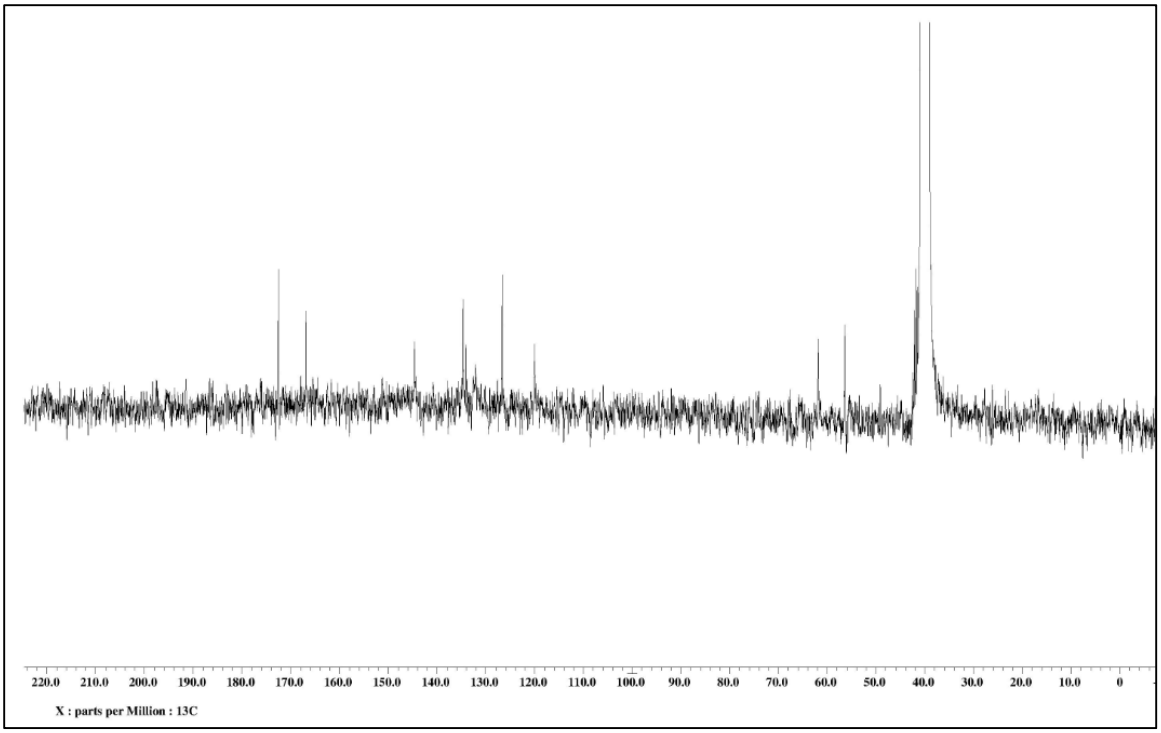

Figure A1.7: ^{13}CNMR spectra for TCPP serine derivative (10).

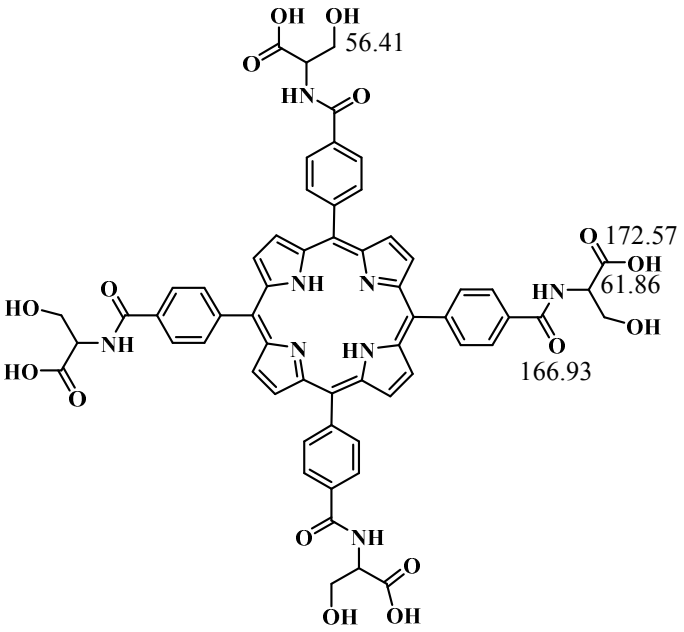

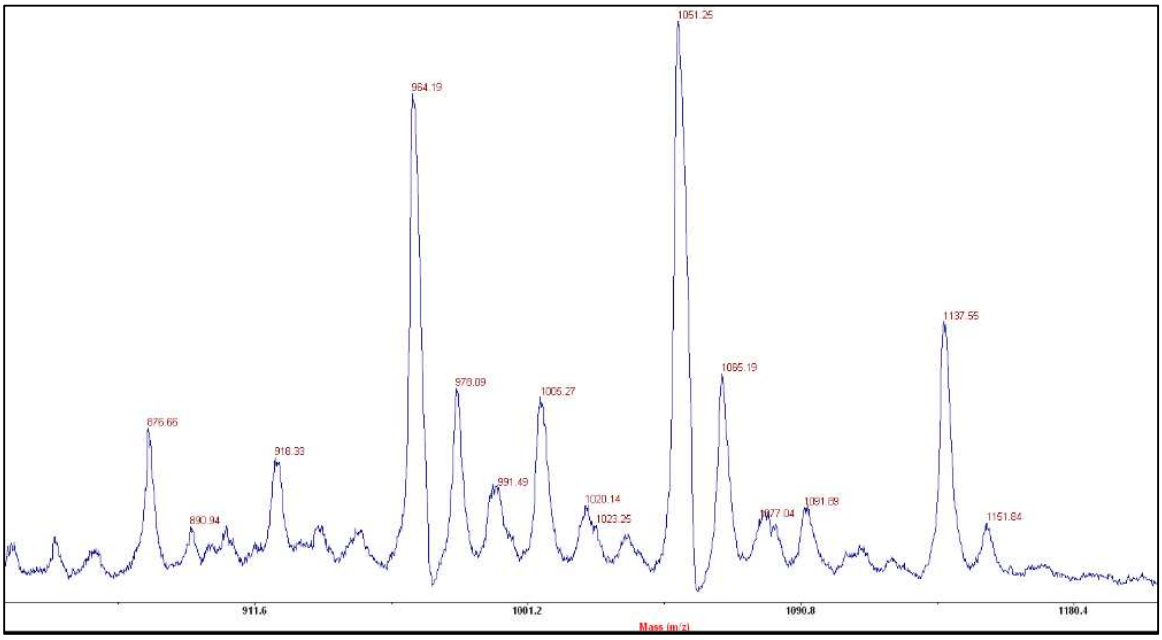

Figure A1.8: MALDI-TOF for TCPP serine derivative (10). M/Z, 1138.70 [M].

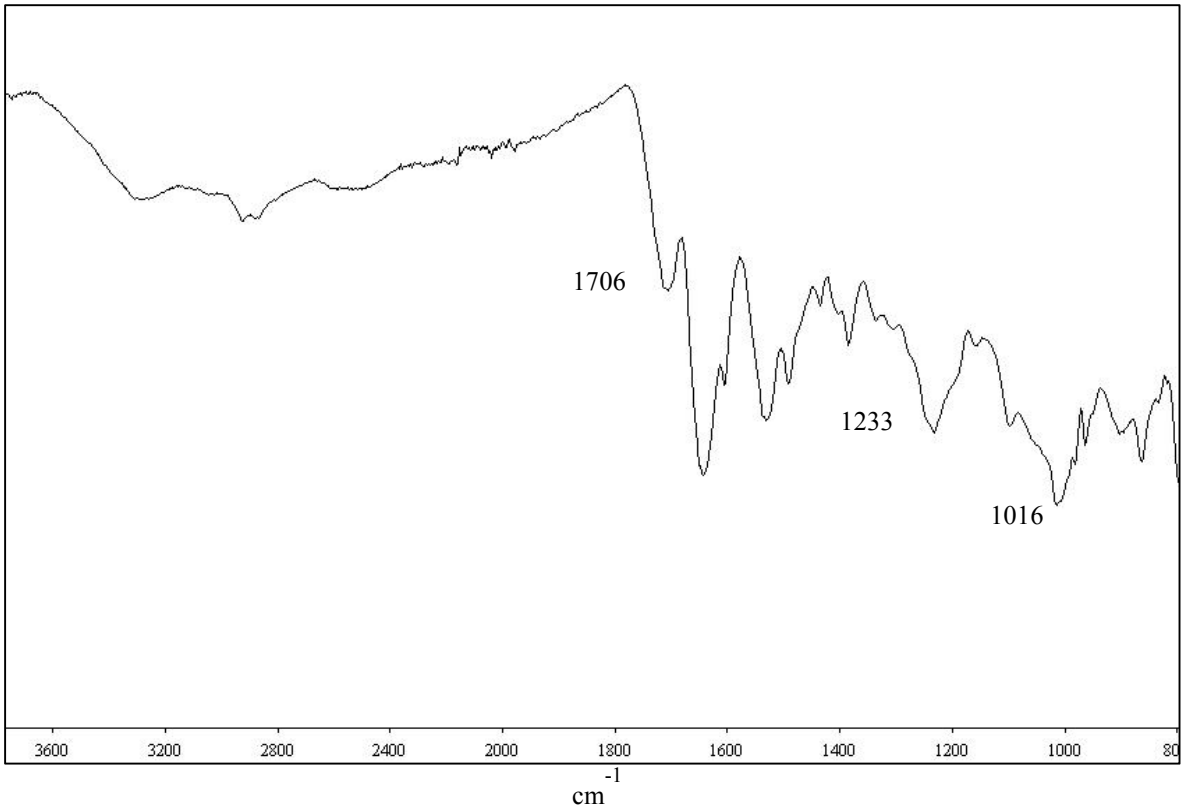

Figure A1.9: FT-IR spectra for control TCPP silane derivative (11). IR: 1016 cm^{-1} (Si-O), 1233 cm^{-1} (Si-C) and 1706 cm^{-1} (carbamate).

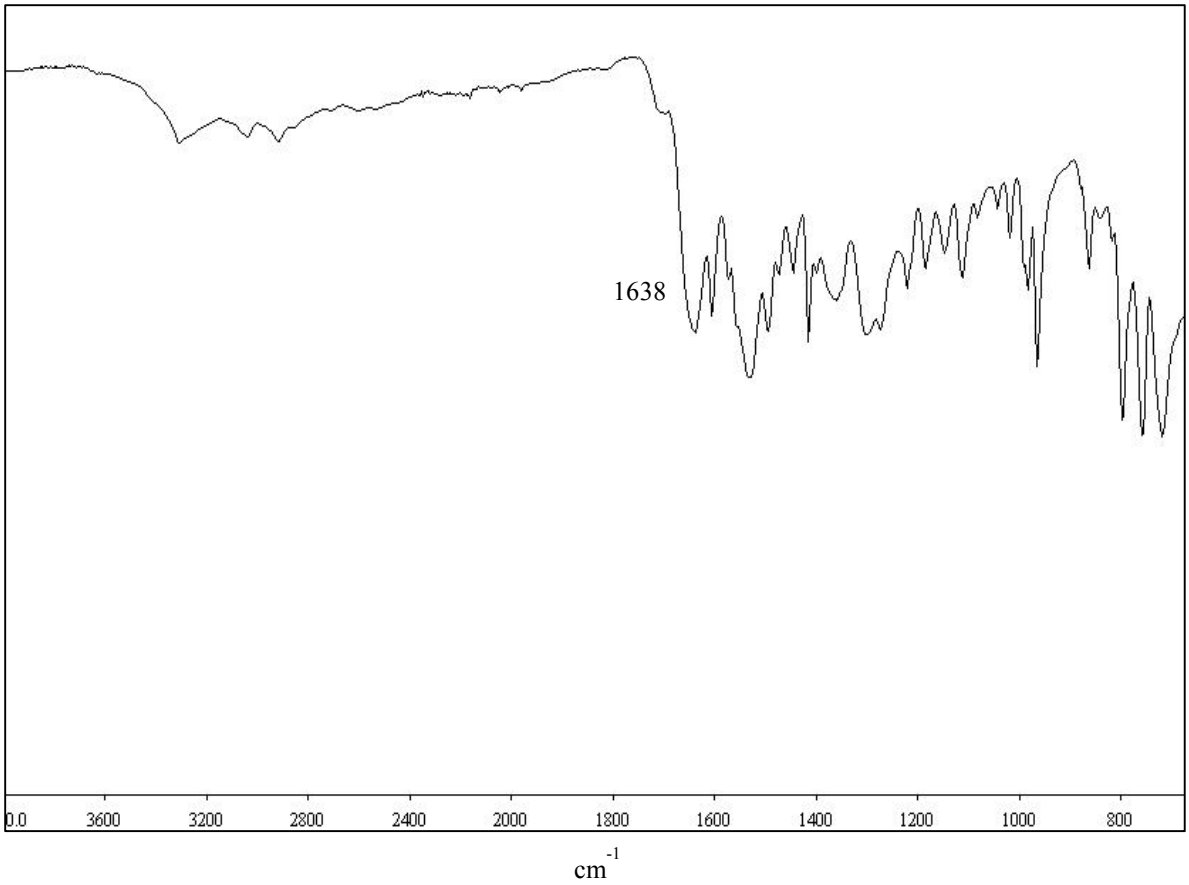

Figure A1.10: FT-IR for pyridine disulfide ethylamine of TCPP (13). IR: 1638 cm^{-1} (amide).

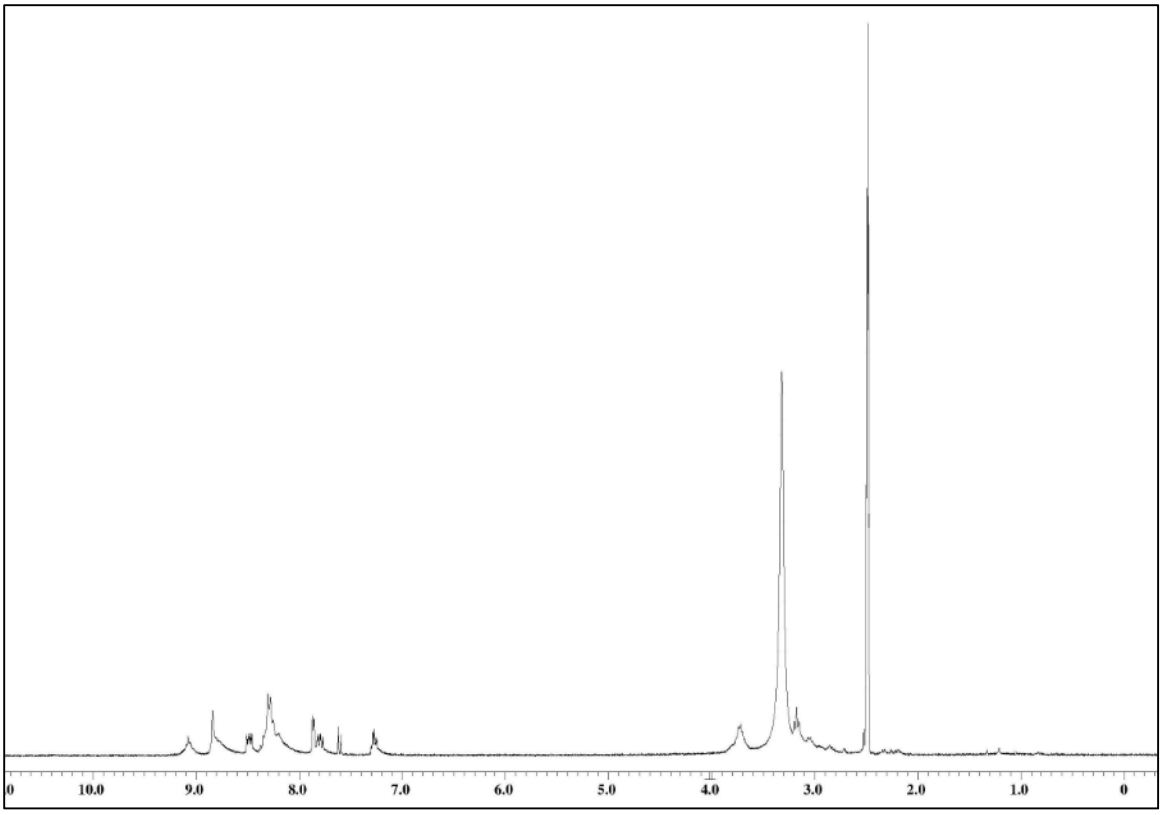

Figure A1.11: ^{1}HNMR spectra for pyridine disulfide ethylamine of TCPP (13).

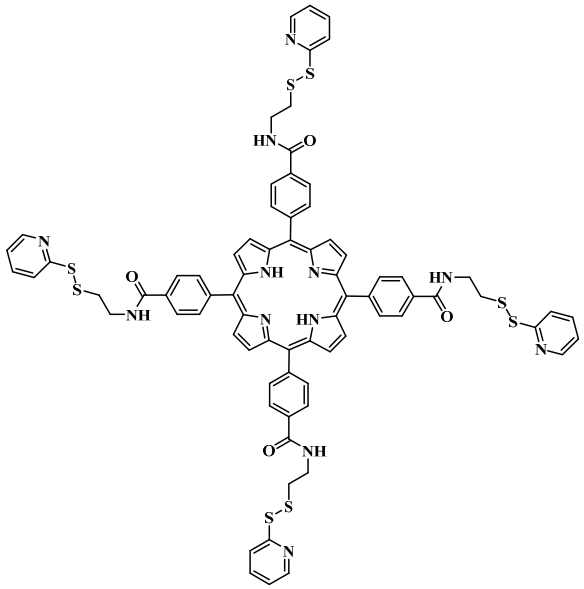

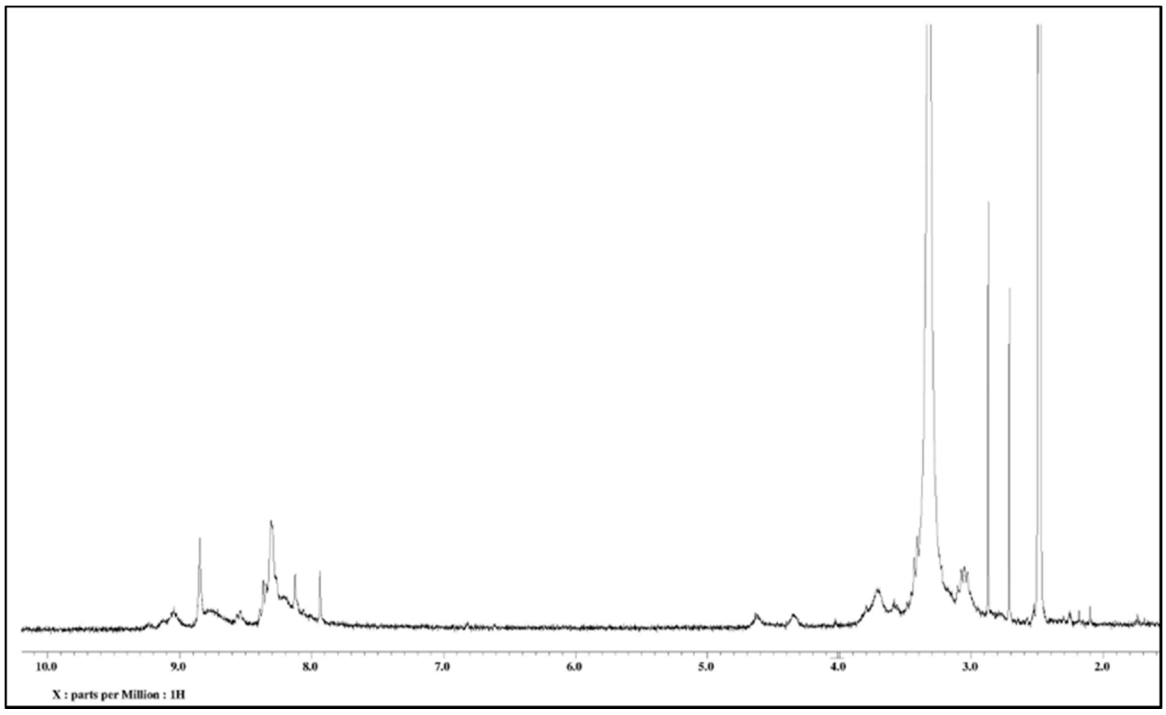

Figure A1.12: [1]HMNR spectra for cysteine disulfide of TCPP (14).

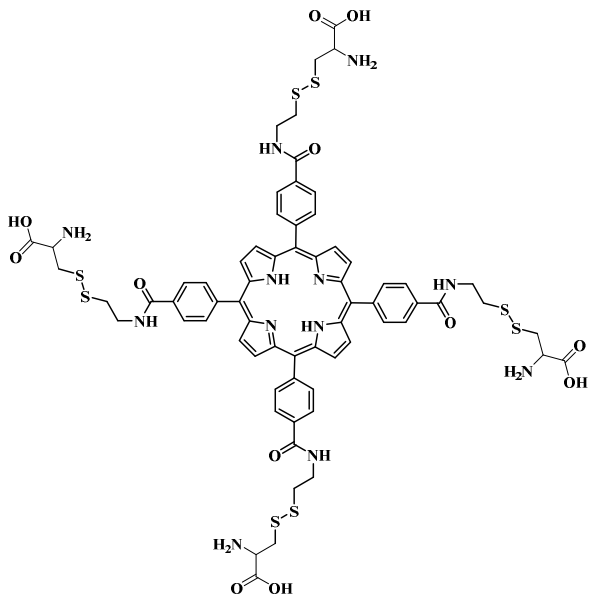

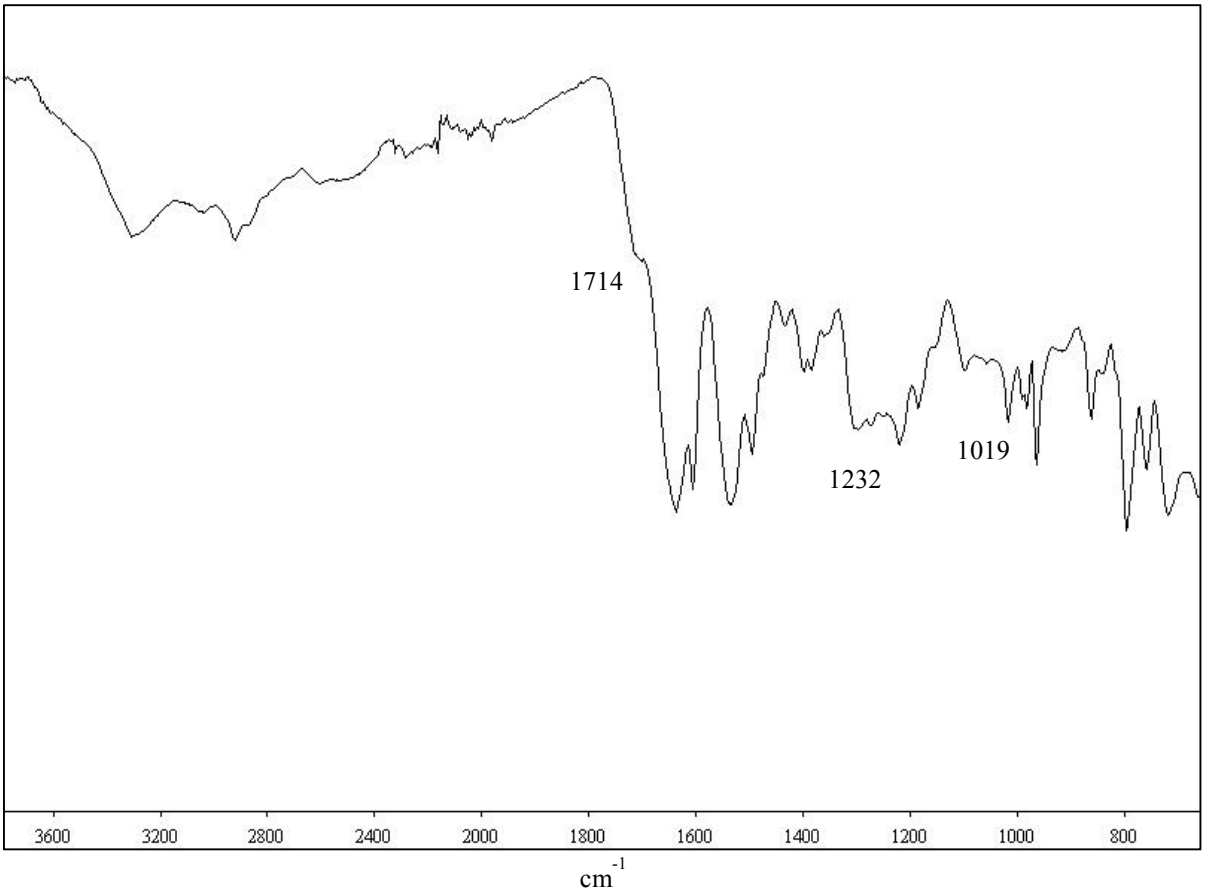

Figure A1.13: FT-IR spectra for redox-responsive TCPP silane derivative (15). IR: 1019 cm^{-1} (Si-O), 1232 cm^{-1} (Si-C) and 1714 cm^{-1} (carbamide).